THE GEOLOGY AND GEOCHEMISTRY OF THE ANSONS BAY BATHOLITH,

N.E. TASMANIA.

Paul A. Kitto, B.Sc., Dip.Ed.

A thesis submitted in partial fulfilment of the requirements for the degree of Bachelor of Science with Honours.

GEOLOGY DEPARTMENT UNIVERSITY OF TASMANIA

December, 1982

ABSTRACT

The granitic complex forming the Ansons Bay Batholith (300 km^2) in northeastern Tasmania, is composed of a variety of granitoids which intrude the low-grade regionally metamorphosed Ordivician to Lower Devonian Mathinna Beds.

The granitoids are divided into five major types based on mafic mineralogy, plagioclase composition and textural variation. Geochemical evidence suggests that the granodiorite, microgranite and biotite-, garnet-biotite, and alkali feldspar granites have been derived by Rayleigh fractional crystallization of a melt from a chemically inhomogeneous source region. Major and trace element modelling of the biotite-, garnet-biotite, and alkali feldspar granites explains the linear trend observed between these granites by 25% fractional crystallization of a solid composed of 64% plagioclase, 20% biotite, and 16% K-feldspar.

Late Devonian dolerite dykes (up to 10 km long) associated with late stage crystallization of the granites, may provide an upper age limit to the Tabberabberan Orogeny within the Ansons Bay Batholith.

An agmatic migmatite, 2 km south of Eddystone Point, has a K-feldspar-cordierite hornfels facies mineral assemblage. P-T conditions of 1 kb and 600° C are inferred for the migmatite formation. Granite contamination and Mathinna Bed xenoliths are largely restricted to the migmatite contact.

Mafic xenoliths from both the granodiorite and garnet-biotite granites have cognate (cumulate) origins and are unrelated to the country rocks. The aplitic xenoliths from the garnet-biotite granites, however, are interpreted as dismembered alkali feldspar dykes.

The mafic mineral assemblages from the garnet-biotite granites suggest low pressure conditions (1 kb) of emplacement at temperatures close to 700^oC. Garnet-biotite (cordierite) geothermometry and feldspar geothermometry confirm these temperatures.

ACKNOWLEDGEMENTS

For their assistance and support, I would like to acknowledge the following people:

Dr Rick Varne, supervisor;

- Drs Neville Higgins, Mike Solomon, Jan van Moort, Ron Berry, Vic Wall, David Ellis and Messrs Ramsay Ford, Ewan Reid, Phil Robinson, and Scott Kuehner for their advice and assistance in their various fields of expertise;
- Steve Hunns, Malcolm Bendel, Peter Bruce, and Phil Viney for their assistance with field work;
- Tiny Le Fevre and Rod Pearce from the National Parks and Wildlife Service for allowing access to and providing free accommodation within Mt William National Park;
- John Denman and family from the Eddystone Point Lighthouse for their hospitality and mechanical assistance.;
- Charlie and Pat Stanley for making available their shack at Ansons Bay;

June Pongratz for typing (and retyping) the manuscript;

All the Honours students for their help and companionship;

Especially my wife Sue, and son Joel, for their patience, understanding and support throughout the year.

CONTENTS

	*			PAGE
	ABST	RACT		i
	ACKN	OWLEDGEMEN	ITS	ii
Chapter 1	INTH	ODUCTION		1
	1.2 1.3	Tectonic Aim of th Previous Present w	ne study work	1 1 3 3
Chapter 2		ONAL SETTI E GRANITOI	NG, GEOLOGY AND PETROGRAPHY OF	4
	2.2	Regional Geology a Granodior	ind petrology	4 6 8
			ardens Pluton Granodiorite Dulder Point Granodiorite	8 13
		Microgran Biotite g		17 19
			asons Bay Biotite Granite Idystone Point Biotite Granite	19 20
	2.7	Alkali fe	otite granites eldspar granite fic and mafic intrusives	22 34 37
		2.8.2 Po 2.8.3 Pe 2.8.4 Mi 2.8.5 Do	olite dykes orphyritic mafic aplite dykes gmatite dykes crogranite dykes olerite dykes mprophyre dyke	37 38 38 38 42 45
	2.9	Intrusive	succession	45
Chapter 3			GRAPHY AND GEOCHEMISTRY OF THE ATITE CONTACT	50
	3.1 3.2 3.3 3.4 3.5	Introduct Structure Petrograp P-T condi migmati	ion of the agmatic migmatite contact by of the agmatic migmatite contact tions of formation of the agmatic te contact stry of the agmatic migmatite	50 50 57 65 68
		3.5.2 Ch	troduction emical variation of the contact migmatite	68 68
			scussion of results	68
	3.6	Summary o	of the agmatic migmatite contact	70

Contents cont.

Chapter 4	GEOLOGY, PETROGRAPHY AND GEOCHEMISTRY OF THE GRANITOID XENOLITHS 71					
	4.1 Introduction4.2 Mafic xenoliths from the granodiorite	71 71				
	4.2.1 Geology and petrography of the mafic xenoliths	71				
	4.2.2 Facies diagrams for the granodiorite mafic xenoliths	73				
	4.3 Mafic xenoliths from the garnet-biotite granite	77				
	4.3.1 Geology and petrography of the mafic xenoliths	77				
	4.3.2 Facies diagrams for the garnet-biotite granite mafic xenoliths	81				
	4.4 Aplitic xenoliths from the garnet-biotite granite	81				
	4.4.1 Geology and petrography of the aplitic xenoliths	81				
	4.4.2 Facies diagrams for the aplitic xenoliths	82				
	4.5 Garnet-biotite (cordierite) rims to xenoliths	83				
	4.5.1 Geology and petrography 4.5.2 Garnet geochemistry	83 85				
Chapter 5	GEOTHERMOMETRY	85				
	5.1 Introduction5.2 Garnet-biotite (cordierite) geothermometry5.3 Feldspar geothermometry	91 91 93				
Chapter 6	GEOCHEMISTRY OF THE ANSONS BAY BATHOLITH	95				
	6.1 Introduction	95				
	6.2 Major element variation	95				
		106 112				
		114				
	6.6 Discussion	117				
Chapter 7	SUMMARY OF CONCLUSIONS	19				
	REFERENCES	124				
Appendix 1		L28				
	5	131				
		L44 L50				
	• • •	166				
	• •	170				
		73				
3F	Microprobe analyses of muscovite	75				
3G	Microprobe analyses of garnet-biotites for					
L	•	.77 .80				
		.00				

CHAPTER 1 INTRODUCTION

1.1 TECTONIC SETTING

The geology of eastern Australia has been influenced by the Palaeozoic Tasman Orogenic Zone. The Lachlan Fold Belt of southeast Australia, in particular, has been dominated by intrusions of Siluro-Devonian granitoids. In Tasmania Devonian plutonism was dominant, and concentrated in northeastern and western Tasmania.

This study concentrates on one section of the plutonic terrain, the Ansons Bay area of northeast Tasmania (Figure 1.1). In this region a variety of granitoids ranging from granodiorite, biotite granite, porphyritic garnet-biotite granite, microgranite and alkali-feldspar granite make up a granitic complex of batholitic proportions (300 km²), hereafter referred to as the Ansons Bay Batholith.

1.2 AIM OF THE STUDY

The aims of this study are:

- To map the boundaries of the various bodies of the Ansons Bay Batholith and establish their field relationships;
- To determine the petrographic and geochemical character of the granitoids and their enclaves; and
- 3) To test various petrogenetic models (fractional crystallization, restite unmixing, and partial melting) for the genesis of the granitoids.

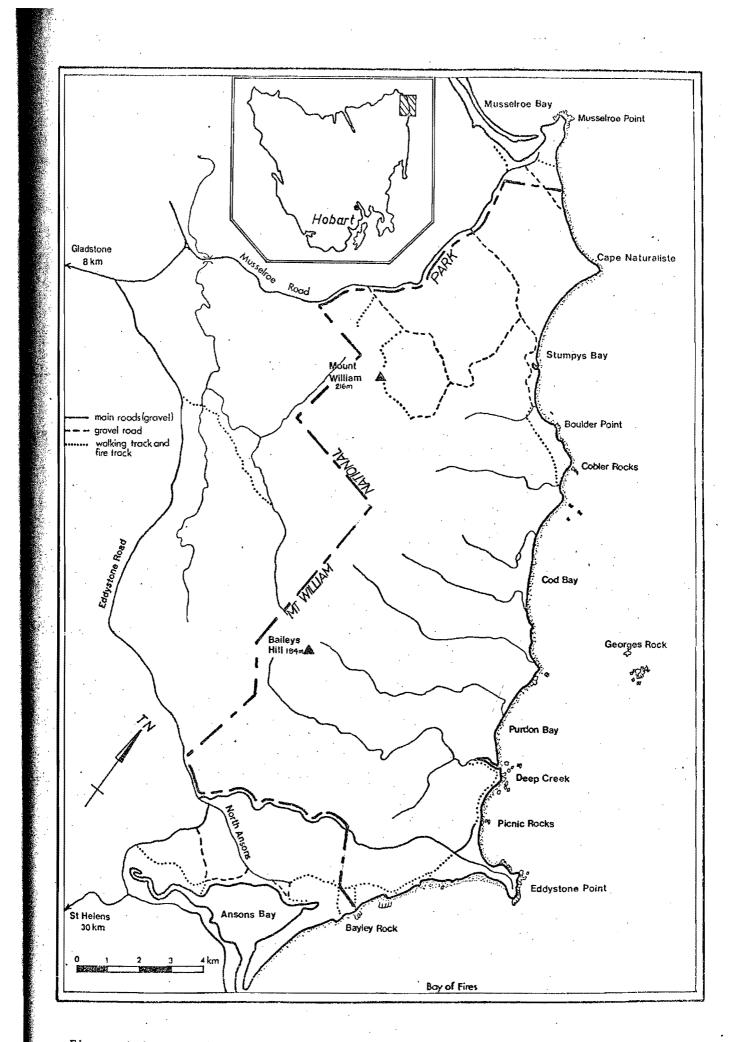


Figure 1.1 Locality map for the Ansons Bay Batholith.

. .

1.3 PREVIOUS WORK

Previous workers have referred to the Ansons Bay Batholith granitoids as the Ansons Bay and Mt William Plutons and included them in the larger composite granitoid mass of the Blue Tier Batholith (Gee & Groves, 1971; Groves, 1972; McClenaghan & Baillie, 1975; Groves, 1977; Jennings, 1977; Groves & McCarthy, 1978; Cocker, 1977, 1981, 1982; McCarthy & Groves, 1979; McClenaghan & Williams, 1982; Higgins et al., in prep.).

The area was mapped previously by Jennings & McShane in 1971, and subdivided into seven different granitoid types. Cocker (1977, 1981, 1982) has since suggested a further subdivision of the eastern Ansons Bay Pluton (Cockers terminology) into north and south zones on the basis of textural variation, biotite and garnet chemistry and Sr isotopic analyses.

1.4 PRESENT STUDY

Work in the field area involved twelve weeks geological mapping and geochemical sampling. Mapping was inhibited by poor access and limited outcrop exposure over much of the area. The uniform vegetation and featureless nature of much of the coastal plain also rendered precise navigation difficult.

Geochemical sampling was concentrated along coastal exposures where deep weathering of the granitoids was limited. Sampling techniques involved knapping, coring, feather and wedge splitting, and blasting depending on the ease of sampling and the extent of outcrop.

CHAPTER 2

REGIONAL SETTING, GEOLOGY AND PETROGRAPHY OF THE GRANITOIDS

2.1 REGIONAL SETTING

The Devonian granitoid plutons of northeastern Tasmania are dated between 395 and 370 Ma (Cocker, 1982). They intrude and contact metamorphose, to low grades, regionally metamorphosed Ordovician to Early Devonian Mathinna Beds (Rickards & Banks, 1979) and are overlain by Middle Sakmarian sediments (Banks, 1962a).

Cocker (1981) interprets the field structures and mineralogy of the contact metamorphic rocks and the granitoids to indicate high levels of intrusion, probably less than 6 km. The steep walled granitoids generally have a north-south elongation, parallel to the regional fold trends of the country rock (Gee & Groves, 1971).

Based on field relationships, petrographic features, and geochemistry (White & Chappell, 1977; Hine et al., 1978; Chappell, 1978) the granitoids in the Ansons Bay Batholith have been classified into I or S types (Table 2.1). The granodiorites are I-type, the microgranite, biotite granite and alkali-feldspar granite are predominantly S-type and the garnet-biotite granites are unquestionably S-type granitoids.

The I-type granodiorites of northeastern Tasmania have initial ⁸⁷Sr/⁸⁶Sr ratios in the range 0.7061 to 0.7073 (Cocker, 1982). The S-type biotite granites have relatively higher initial ⁸⁷Sr/⁸⁶Sr ratios (0.7070-0.7015) which overlap with those of the I-type granodiorites. The S-type garnet-biotite granites (Ansons Bay) have initial ratios greater than 0.7119, indicative of enriched, high Rb/Sr ratio, crustal source-rocks of Proterozoic age (1700-800 Ma). The hydrothermally altered alkali-feldspar granites have poorly constrained initial ratios due to an open Sr isotope system. The range in initial ⁸⁷Sr/⁸⁶Sr ratios

TABLE 2.1 \pm 1 vs. S discriminants and features of the Ansons Bay Batholith

and the second second

1 21 1

granitoids,

			Granodierite		Riotite GL-blot granite granite					
	І-ТҮРЕ	S-TYPE	Gardens	Boulder Point	Musselroe Point Microgranite	Änsons Bay	Eddystone Point	Porphyritic	Coarsely porphyritic	Alkalî feldspar granite
	FIELD RELATIONSHIPS	5	···· ··· ···							* 2008 - C
1	Commonly older than associated S-types.	May intrude I type.	?	?	S	?	?	?	?	?
2	Very rarely associated with a regional metamorphic aureole.	May be associated with a regional metamorphic aureole.	I	I	?	?	? `	?	.?	?
3	Amphibole-bearing xenoliths common.	Very rare amphibole-bearing xenoliths.	I	I	s	S	\$	s	S	S
4	Sedimentary xenoliths very rare, confined usually to pluton margins.	Often abundant recrystallized sedimentary xenoliths, throughout.	I	I	I	I	S	S	S	I
5	Massive or with primary foliation.	Often strongly secondary foliation.	I	I	I	I	I	I	I	I
6	PETROGRAPHIC FEATURES Hornblende common in mafic types but may be absent from very felsic types.	No hornblende.	I	I	S	s	s	S	S	S
7	No primary muscovite.	Muscovite common in felsic types.	,Ι	I	s	\$	S	S	S	S
8	Biotite <15 modal %.	Up to $\sim 30\%$ biotite in mafic variety.	I	I	\$ ·	s	S	s	s	S
9	Sphene or allanite are common accessories.	No sphene, uncommon allanite.	I	I	S	S	\$	s	S	S,
10	Accessory monazite uncommon.	Accessory monazite common.	1	I	\$	s	S	S .	s	Ι.
11	No aluminosilicates, garnet or cordierite.	Aluminosilicates, garnet or cordierite present in xenolith- rich varieties.	I	, I	S	I	I	S	ŝ	I
12	Apatite only as inclusions.	Apatite as discrete, often relatively large crystals.	I	I	S	\$	S	s	S	S
13	Magnetite and ilmenite as oxide phases.	Magnetite rare, ilmenite the common oxide phase.	·I	S	\$. S	S	s	s	S
14	<u>CHEMISTRY</u> Suites have broad composition ranges mafic to felsic.	Suites have restricted composition ranges.	I	ľ	s	\$ ^r	s	S	s	S
15	High degree of linear inter-element correlation on variation diagrams.	Variation diagrams more scattered.	I	I	S	\$	S	S	S	S ,
16	Na ₂ O always >1.8%, may be >3.5%.	Na ₂ O always <3.3%, may be <1.8%.	I	I	I	S	I	\$	S	I,S
17		Sr usually <200 ppm.	I	I	S	\$	S	S	S	S
18	$Mol\left(\frac{Al_{2}O_{3}}{Na_{2}O+K_{2}O+CaO}\right) < 1.1$	$Mol\left(\frac{Al_{2}O_{3}}{Na_{2}O+K_{2}O+CaO}\right) > 1.1$	I	I	1,5	I	I	s	S	S
19	CIPW normative diopside or <1% normative corundum.	>1% normative corundum.	I	I,S	S	I	I	5	S	S
20	(⁸⁷ Sr/ ⁸⁶ Sr)。0.704-0.706, good isochrons.	(⁸⁷ Sr/ ^{8€} Sr)₀ >0.708, often poor isochrons.	I	I	?	1,5	Ι,S	s	S	?
21	δ ¹⁰ 0 < 9.5%	$\delta^{18}0 > 9.9\%$?	?	?	?	?	?	?	?
22	δD often < -69%	δD > -69%	?	?	?	?	?	?	?	3

of the granitoids from 0.7061 to 0.7136 has led Cocker (1982) to conclude that each granitoid had a characteristically different protolith composition.

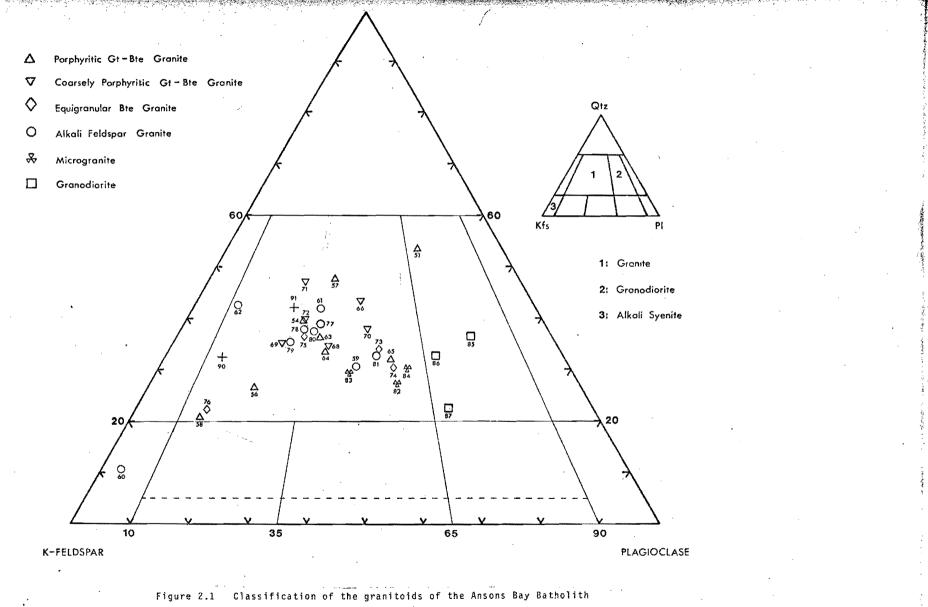
Biotite ages (Cocker, 1982) for the Gardens Granodiorite and the garnet-biotite granite of north Ansons Bay are 383 and 375 Ma respectively. Compositional variations in coexisting garnet and biotite (Cocker, 1981) suggests subdividing the garnet-biotite granite into northern and southern portions. Two reasonable isochron fits are also interpreted as separate intrusions of different initial ratios (Cocker, 1982).

2.2 GEOLOGY AND PETROGRAPHY

Jennings (1977) has established a succession for the Ansons Bay area consisting of a Mathinna Bed basement, a series of granitic intrusions and a copious blanket of Tertiary to Recent sands, gravels, and alluvial deposits. Doleritic and leucocratic dykes succeeded the major granitoid intrusions probably in Late Devonian times, followed by a lamprophyric intrusion (dyke) of probable Cretaceous age, and a basalt similar to northeastern Tasmanian Tertiary basalts.

In this study the granitic rocks of the Ansons Bay Batholith have been subdivided on the basis of (i) the mafic mineralogy, (ii) the plagioclase composition, and (iii) the textural variation (after Higgins et al., 1982). Nomenclature is based on modal analyses (Figure 2.1 and Appendix 1) and follows the outline of Streckeisen (1976).

The granitic subdivisions are:



according to Streckeisen (1976).

÷.,

- 1. Granodiorites
 - (a) Gardens Pluton Granodiorite
 - (b) Boulder Point Granodiorite

2. Microgranites

- 3. Biotite granites
 - (a) Ansons Bay
 - (b) Eddystone Point
- 4. Garnet-biotite granites
 - (a) porphyritic
 - (b) coarsely porphyritic
- 5. Alkali-feldspar granites (Mt William)

2.3 GRANODIORITES

Two distinctly different biotite hornblende granodiorites outcrop within the Ansons Bay Batholith. The first is a medium grained equigranular biotite-hornblende granodiorite (Gardens Pluton Granodiorite), and the second, a porphyritic medium-coarse grained biotite-hornblende granodiorite (Boulder Point Granodiorite).

2.3.1 Gardens Pluton Granodiorite

A dark grey, massive, medium grained, equigranular biotitehornblende granodiorite containing 15-25% mafic minerals outcrops in the southwest corner of the Ansons Bay Batholith (Figures 2.2, 2.3). Outcrop occurs as very poorly exposed, low whale back formations confined to the wooded valley of Icena Creek and its tributaries.

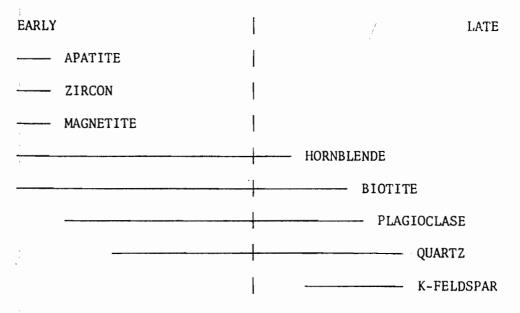
Jennings and McShane (1977) have inferred that the granodiorite extends southeastwards beneath Tertiary sediments to join the main body of the Gardens Pluton. Contact relationships with the garnet-biotite granites and Mathinna Beds to the east and northeast respectively are obscured, but the 1.0 to 1.5 km wide contact metamorphic aureole in the Mathinna Beds is attributed to the intrusion of a large igneous body such as the Gardens Pluton Granodiorite (P. Baillie, pers. comm., 1982; Figure 2.3).

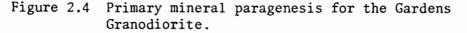
The petrographic features for the Gardens Pluton Granodiorite are summarized in Table 2.2. Briefly, they consists of subhedral to euhedral reversed oscillatory zoned labradorite (cores An₅₂, rims An₅₇), subhedral to euhedral dark brown biotite and euhedral green hornblende, forming composite grain aggregates in places, with interstitial microcline (Plate 2.1). Quartz occurs as discrete grains, commonly undulose, or annealed to a fine grained mosaic of polygonal subgrains.

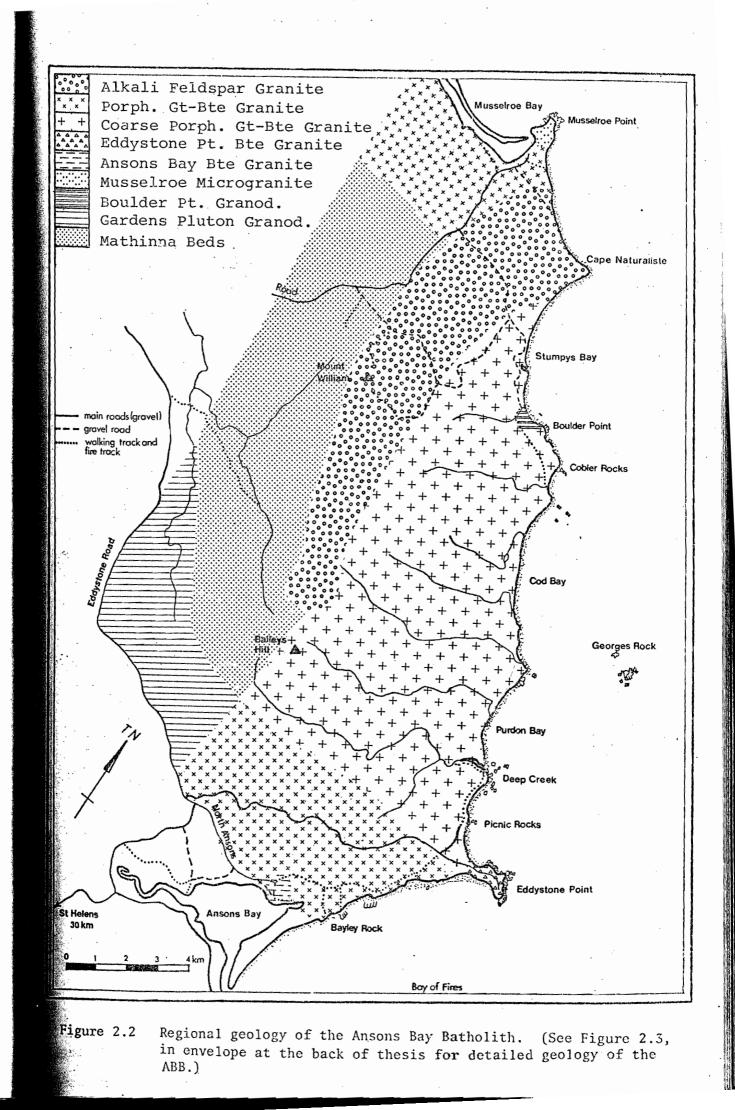
Petrographic evidence suggests the early crystallization of hornblende, biotite, plagioclase and some quartz with late crystallization of K-feldspar together with additional quartz.

The increase in calcium from core to rim in plagioclase may be the result of (i) a sudden pressure release, possibly intrusion, or (ii) a cessation of hornblende crystallization (not supported petrographically). The primary mineral paragenetic sequence for this rock type is presented in Figure 2.4.

TIME OF EMPLACEMENT







PHASE	GRANODI	ORITE	BIOTITE GRANITES			
FIASE	GARDEN PLUTON	BOULDER POINT	ANSONS BAY	EDDYSTONE		
QUARTZ	<pre></pre>	<pre><3num anhedral grains, interstitial or forming aggregates <15num. Inclusions of zoned zircon, and all major phases except horn- blende.</pre>	Equant anhedral grains (3mm with weak undu- lose extinction. Inclusions of biotite, plag and apatite.	Anhedral interstitial phase (4mm with weak undulose extinction. Inclusions of biotite plag, K-felspar, apatite and zircon.		
BIOTITE	<pre><2mm columnar grains. Deep brown,or green if chloritic alteration. Slightly bent with minor apatite, zircon and qtz inclusions.</pre>	(Amm equant grains, dark brown with minor K-felspar replacement. Accessory minerals include apatite, mona- zite, zircon + quartz.	<1.5mm subhedral col- umnar and lath forms. Dark brown with some minor green chloritic alteration. Metamict biotites have embayed edges with feldspars. Acc. include apatite, monazite + ilmenite.	<pre>{2mm subhedral columna forms. Dark brown, minor embayment of metamict biotites, and quartz, and inclusions of apatite, monazite and zircon.</pre>		
K-FELSPAR	<pre><3mm anhedral grains, undulose extinction, with inclusions of biotite and plagio- clase. Interstitial.</pre>	Phenocrysts (<30mm) & in grdmass as (<3mm) anhedral grains; with undulose extinction. Inclusions of zircon, sphene, qtz, plag,bte, hornblende (handsp. has phenocrysts).	Anhedral equant forms <pre></pre>	Anhedral equant forms. (4mm commonly inter- stitial. Occurs as microperthites of orthoclase. Inclusion of quartz + minor biotite and plagioclas		
PLAGIOCLASE	\$3.5mm euhedral to subhedral columnar grains, oscillatory zoning (cores An52, rim An57) with cloudy cores. Some Carlsbad- albite and pericline twinning.	<pre>(10mm eunedral-sub- hedral equant grains with oscillatory zon- ing (cores An₆₀, rim An₇₀). Carlsbad-albite and pericline twinning often curved. Myrme- kitic and reversed twinning of margins in contact with K-fels & within some zoning. Inclusions of stannite?, hornblende & zircon.</pre>	Euhedral to sub- hedral columnar forms (3mm. Oscillatory zoned (cores An53-An10) showing Carlsbad-albite and pericline twinning. Myrmekitic and reversed twinning of margins in contact with K-felspar	showing albite, Carlsbad-albite and pericline twinning. Sericite defines		
MUSCOVITE	absent	absent	Minor phase after sericite in plagio- clase cores.	absent		
AMPHIBOLE	<pre><3mm euhedral-sub- hedral columnar grains. Deep green pleochroism and magnetite inclusions Some quartz embay- ment and alteration to rims.</pre>	<pre>\$\lambda \lambda \lam</pre>	absent /	absent		
CHLORITE	Minor subparallel fracture-cleavage fillings (<0.15mm) of biotite.	absent	Minor subparallel fracture-cleavage fillings (<0.1mm) of biotite.	absent		
GARNET	absent	absent	Occurs as minor phase in handsp. as 1 mm rose- coloured crystals.	absent		
CORDIERITE	absent	absent -	absent	absent		
APATITE	Acicular crystals (<0.lum) within biotite.	Small acicular crystals (<0.3mm)within all major phases.	Small acicular crystals (<0.2mm) in biotite and quartz.	Acicular crystals and prisms(<0.1mm) in quartz, biotite and plagioclase.		

Table 2.2 Petrographic features of the granitoids from the Ansons Bay Batholith.

Table 2.2 (continued)

PHASE	MUSSELROE	GARNET-BIOTIT	ALKALI			
	POINT MICROGRANITE	PORPHYRITIC	COARSELY PORPHYRITIC	FELDSPAR GRANITE		
QUARTZ	(1.5mm interlocking anhedral grains with undulose extinction. Inclusions of all major phases plus accessory apatite and zircon.	Anhedral equant grains (Gmmn with weak undulose extinction. Simultaneous crystallization with K-fels. Inclusions of biot, plag, K-fels and apatite.	weak to absent undulose	Minor anhedral equant to n elongate grains (5mm)with e well developed undulose s extinction. Inclusions of plag, biot(altered) and zircon.		
BIOTITE	<pre>Kimmsubhedral laths assoc. with cordierite clots. Brown with green chloritic or quartz replacement. Acc. minerals of apatite, monazite, quartz and ilmenite.</pre>	<pre><damm cquant<br="" cuhedral,="">to columnar forms with dark brown colouring. Usually forms aggre- gates <8mm. Contains inclusions of apatite, monazite, biotite, plus minor ilmenite and zircons. Minor green chloritic and muscovitic alteration is present.</damm></pre>	<pre><dum euhedral="" sub-<br="" to="">hedral columnar forms with dark brown colour- ing. Usually forms aggregates < Sum. Contains inclusions of apatite, monazite, biotite + minor ilmenite & zircons. Minor green chloritic alteration present.</dum></pre>	Anhedral laths <2mm, brown with alteration to pale brown biotite and muscovite. Remnant pleochroic haloes but no obvious accessory minerals.		
K-FELSPAR	Sparse subhedral pheno- crysts up to 12mm, grd mass usually <2mm, Phenocrysts simply twinned, grd mass has undu lose extinction. Phenocryst has micro- antiperthite exsolu- tion and inclusions of biotite, K-fels, plag, muscovite & needles of apatite.	Phenocrysts (<30mm) and in the grd mass (<2mm) as anhedral to sub- hedral equant forms with slight undulose extinc- tion. Occur as ortho- clase and microcline microperthites with inclusions of biotite, apatite, plag, vermicular quartz and replacement muscovite.	ganglion forms. Occur as replacement micro- cline and orthoclase microperthites with inclusions of grano-	Anhedral equant micro- perthite forms <4mm, with inclusions of plag, quartz, and biotite. Muscovite and sericite alteration prevalent.		
PLAGIOCLASE	<1.5mm subhedral equant to columnar grains with slight zoning (core Ang2-rim An11) and seri- citized cores. Albite and Carlsbad-albite twinning. Myrmekitic and reversed twinning of margins in contact with K-fels. Minor inclusions of apatite and biotite.	equant forms <4mm. Oscillatory zoned (core An45-rim An20) showing	sericitized cores and	equant forms with little zoning (core Ang-rim An ₂). Exhibit Carlsbad-		
MUSCOVITE	Anhedral flakes re- placing biotite, K-fels and sericite in cordierite.	Minor anhedral flakes replacing biotite, K-fels and sericite after plagioclase.	Minor anhedra∦ flakes replacing biotite, K-fels and sericite after plagioclase.	Anhedral flakes replacing biotite, K-fels and sericite after plagioclase.		
AMPHIBOLE	absent	absent	absent	absent		
CHLORITE .	Complete replacement of biotite or sub- parallel fracture- cleavage fillings. Possible replacement of sericite after cordierite.	Fracture-cleavage fillings, <1.5mm. Acicular needles of iron carbonate present within chlorite.	Fracture-cleavage fillings((I.Cmm) of biotite.	absenț		
GARNET	absent	Euhedral to anhedral forms <10mm in inter- growths with brown biotite and cordierite.	Euhedral to anhedral forms <10mm in inter- growths with brown biotite.	absent		
CORDIERITE	2nm rhombs partially replaced by biotite, sericite, chlorite & muscovite. Minor needles of apatite.	<pre><5mm rhombs partially replaced by sericite and intimately inter- grown with biotite and garnet.</pre>	not observed	absent		
APATITE	Small acicular crystals(<0.2nm)in all major phases.	Small acicular crystals(<0.1mm) in all major phases.	Small acicular crystals(<(k.Vew)in biotite.	absent		

. .



Plate 2.1 Petrographic features of the Gardens Pluton Granodiorite.

Point counting of stained slabs and thin sections of the Gardens Pluton granitoid (#63085) found it to plot inside the granodiorite field of Streckeisen (1976) (Figure 2.1).

2.3.2 Boulder Point Granodiorite

A foreshore exposure of a grey, coarse-medium grained porphyritic biotite-hornblende granodiorite occurs 5 km east-northeast of Mt William at Boulder Point (Figures 2.3, 2.5). This previously unmapped unit locally exhibits an incipient foliation etched by wind and wave action producing a characteristic fluted surface (Plate 2.2). The planar arrangement of K-feldspar megacrysts and mafic xenoliths imparts a primary (?) mineral foliation trending approximately 325^oN.

Petrographic features, summarized in Table 2.2, include microcline, microperthite phenocrysts up to 40 mm, euhedral to subhedral reversed oscillatory zoned labradorite (cores An_{60} , rims An_{70}), subhedral to euhedral dark brown biotite and subhedral green hornblende, forming composite grain aggregates. Interstitial orthoclase exhibits a myrmekitic texture against plagioclase margins (Plate 2.3), and quartz grains are undulose.

Petrographic evidence suggests a similar crystallization to the Gardens Pluton Granodiorite, with the exception that poikilitic K-feldspar phenocrysts began crystallizing earlier. The suggested primary mineral paragenetic sequence for the Boulder Point Granodiorite is illustrated in Figure 2.6.

Modal analyses of the Boulder Point granitoid (#63086, #63087) classify it as a granodicrite (Figure 2.1) according to Streckeisen (1976).

Two types of mafic xenoliths with smooth ovoid shapes aligned parallel to the K-feldspar mineral foliation are found within the granodiorite. The most abundant xenoliths have a hornblende-biotiteplagioclase composition. Other xenoliths contain plagioclase megacrysts in a plagioclase-biotite-hornblende groundmass.

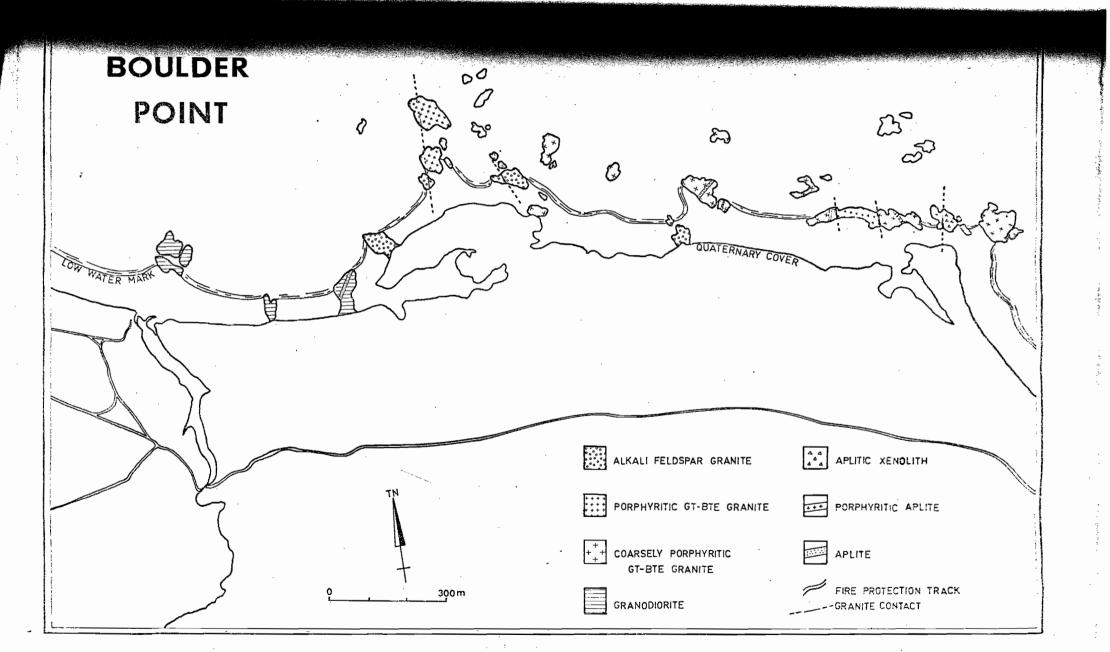


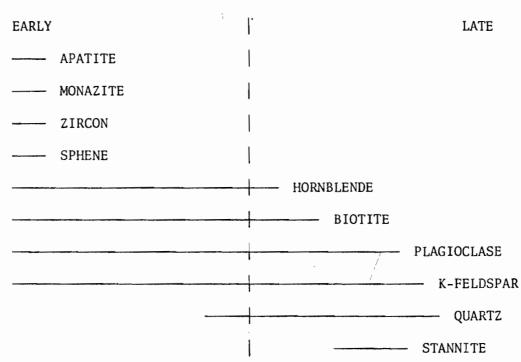




Plate 2.2 Boulder Point Granodiorite with an incipient foliation etched by wind and wave action to produce a characteristic fluted surface.



Plate 2.3 Petrographic features of the Boulder Point Granodiorite.



TIME OF INTRUSION



Figure 2.6 Primary mineral paragenesis for the Boulder Point Granodiorite.



Plate 2.4 Sinuous trains of K-feldspar megacrysts penetrating the fine grained Musselroe Point Microgranite.

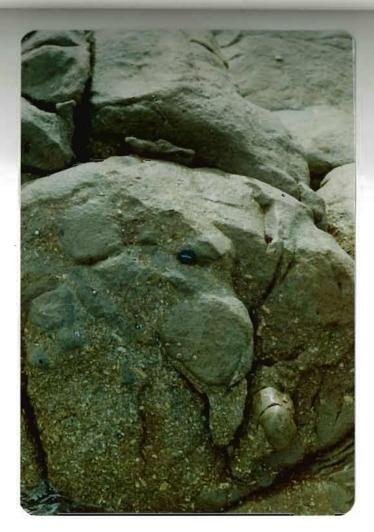


Plate 2.5 Field relationships betweem the porphyritic garnet-biotite granite and microgranite interpreted as the incomplete mixing of two contemporaneous melts of differing viscosities.

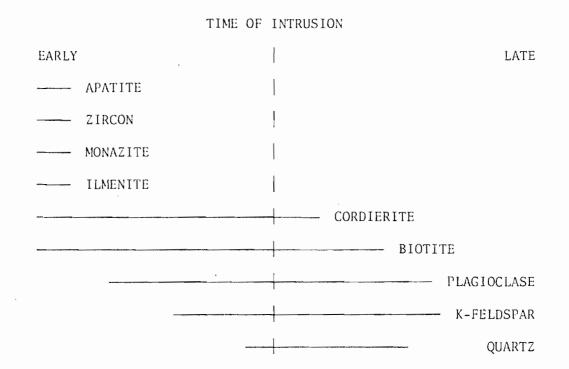


Figure 2.7 Primary mineral paragenesis for the Musselroe Point Microgranite.

Modal analyses of the Musselroe Point granitoid (#63083, #63084) classify it as a granite (Figure 2.1) according to Streckeisen (1976)

2.5 BIOTITE GRANITES

Two texturally distinct equigranular biotite granites occur within the Ansons Bay Batholith. The first is a medium grained biotite granite outcropping on the north shore of Ansons Bay. The second, a medium to fine grained biotite granite, is exposed at Eddystone Point.

2.5.1 Ansons Bay Biotite Granite

A dark grey, massive, fine-medium grained biotite granite outcrops on the north shore of Ansons Bay against a porphyritic garnet-biotite granite (Figure 2.2). The contact is poorly exposed at the low tide mark, is severely weathered, and relative ages can not be assigned. Quaternary sands cover most of the area, with reasonable outcrop being restricted to the shoreshore. Table 2.2 summarizes the petrographic features of this biotite granite. Briefly, it is composed of euhedral to subhedral oscillatory zoned andesine-oligoclase (cores An_{53} , rims An_{10}), subhedral dark brown biotite, weakly undulosing quartz grains, and an interstitial microcline microperthite (Plate 2.6). The primary mineral paragenetic sequence suggested from the petrography are early crystallizing biotite, then plagioclases, quartz and finally K-feldspar (Figure 2.8).

TIME OF INTRUSION

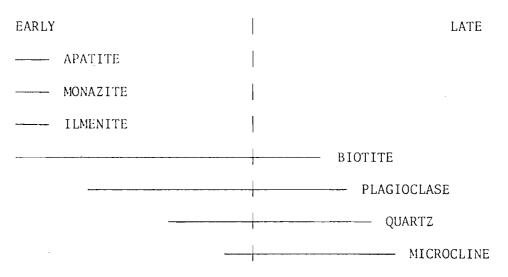


Figure 2.8 Primary mineral paragenesis for the Ansons Bay biotite granite.

A modal analysis of the Ansons Bay biotite granite (#63073, #63074) classify it as a granite (Figure 2.1) according to Streckeisen (1976).

2.5.2 Eddystone Point Biotite Granite

A light grey, massive, mediun to fine grained biotite granite outcrops around the shoreline of Eddystone Point.

A petrographic study (Table 2.2) shows that the plagioclase has oscillatory zoning (cores An_{39} , rims An_8), the dark brown biotites are subhedral, the quartz grains are weakly undulosed and the interstitial orthoclase is microperthitic (Plate 2.7).



Plate 2.6 Petrographic features of the Ansons Bay Biotite Granite.



Plate 2.7 Petrographic features of the Eddystone Point Biotite Granite.

The primary mineral paragenetic sequence for the major phases is identical to the Ansons Bay biotite granite (Figure 2.8). The accessories differ in that zircon and apatite are now abundant as early phases.

Two kilometres southwest of Eddystone Point and in contact with the Mathinna Beds is a rock which has a chilled granitic texture but which is still similar to the Eddystone Granite. Comparable mineralogical compositions lend support to this observation and suggests the southwest exposure to be part of the Eddystone Point granite. A similar chilled granitic texture associated with Mathinna Beds has been found 750 m along Deep Creek some 5 km northwest of Eddystone Point.

Thin section (#63075) of the granite south of Eddystone Point provides evidence of biotite, plagioclase, quartz and orthoclase phenocrysts coexisting in the liquid prior to intrusion (Plate 2.8).

Modal analyses of the Eddystone Point granitoids (#63075, #63076) classify the rock type as a granite (Figure 2.1) according to Streickeisen (1976).

2.6 GARNET-BIOTITE GRANITES

The porphyritic garnet-biotite granites constitute the major rock unit of the Ansons Bay Batholith, extending from Ansons Bay in the south to Musselroe Point in the north. The north-south trending western margin contact-metamorphoses the Mathinna Beds in the south and abuts the alkali feldspar granite further to the north, before becoming intimately associated with the microgranite at Musselroe Point (Figure 2.2).

Jennings (1977), previously divided the garnet-biotite granite of the Ansons Bay Batholith into eastern and western regions on textural evidence. Recent mapping would refute such a division and instead proposes a north-south subdivision of the granitoid east of Eddystone

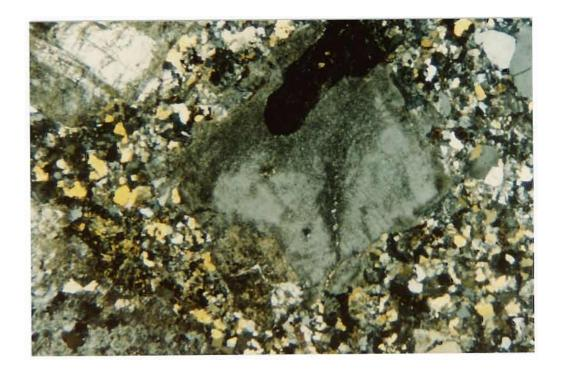


Plate 2.8 Petrographic features of the Eddystone Point Biotite Granite at its contact with the Mathinna Beds. Point. This division is further supported by biotite and garnet geochemistry together with Sr isotopic analyses (Cocker, 1977, 1982).

Typical outcrops consist of low granite tors littered with crumbling boulders several metres in diameter. The deeply weathered inland exposures are buff in colour and iron stained, whereas the fresher coastal material is grey in colour with a local incipient foliation etched by wind and wave action producing characteristic fluted surfaces (Plate 2.9a,b).

Structurally, the planar arrangement of K-feldspar megacrysts and xenoliths form an arcuate north-south mineral foliation around the batholith approximately perpendicular to the leucocratic dykes (Figure 2.9). Pitcher & Berger (1970) suggest that in general a K-feldspar foliation reflects an imposed stress field during the later stages of intrusion and crystallization of a pluton.

Biotite schlieren (Plate 2.10a) and biotite-K-feldspar-rich layers indicate that during crystallization areas of the magma underwent convection (R. Berry, pers. comm., 1982). If shearing is restricted to narrow boundaries it will effectively differentiate the magma (Bagnold Effect) separating the finer grained biotites from the K-feldspar phenocrysts (Plate 2.10b), i.e. the reverse grain size graded layers are due to a variation of grain-dispersive pressure with shear at the margins of the flow (Barriere, 1981).

Rare miarolitic cavities containing tourmaline, K-feldspar, quartz, biotite and muscovite occur in a number of areas.

At Boulder Point (grid ref. FQ059724) the apparent roof of a $c_{i,j,k} = f_{i,j,k}$ sparsely porphyritic alkali feldspar granite outcrops through a coarsely porphyritic garnet-biotite granite (schematic diagram - Figure 2.10). A mono-mineralic layer of K-feldspar 0.5 m thick and associated with miarolitic cavities, plus a volatile-rich dyke form the roof of the intrusive. This layer grades downward into a sparsely porphyritic



Plate 2.9(a) Coarsely porphyritic garnet-biotite granite with an etched fluted surface, a result of wind and wave action.



Plate 2.9(b) An aplitic xenolith within the garnet-biotite granite. The incipient foliation on the surface of the xenolith has resulted from wind and wave action.

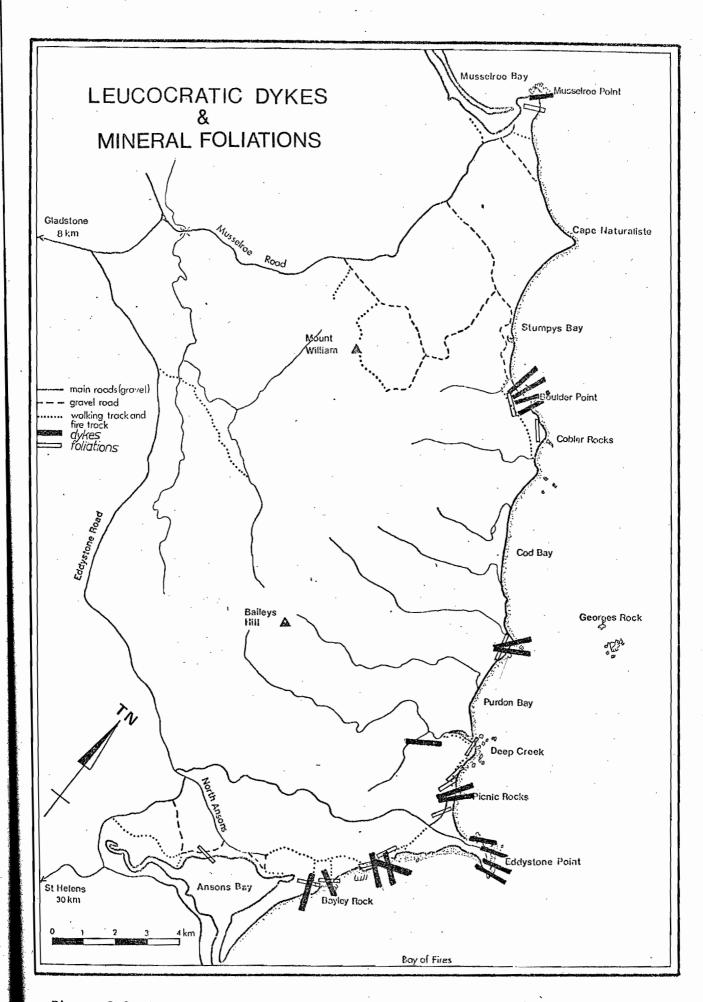


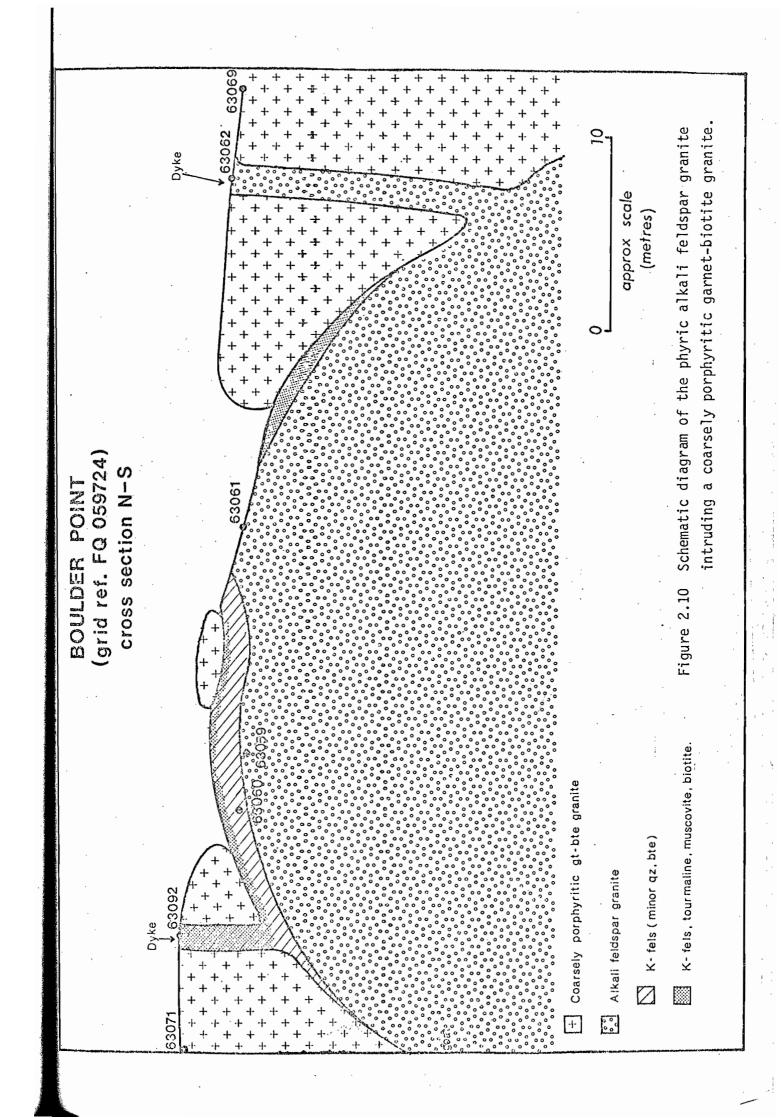
Figure 2.9 Arcuate nature of the mineral foliation perpendicular to the leucocratic dykes within the Ansons Bay Batholith.



Plate 2.10(a) Biotite schlieren within the garnet-biotite granite, indicative of magmatic convection.



Plate 2.10(b) Biotite-K-feldspar rich zone, resulting from Bagnold Effects within the magma.



alkali feldspar granite at depth. The two porphyritic granites are chemically related (#63071, #63061) suggesting that the intrusion represents a localized remobilization of volatile-rich magma within a parent chamber.

Xenoliths are common in the garnet-biotite granites (1-2%) and include both sedimentary and igneous (cognate) varieties. The xenoliths are dealt with in a later chapter.

Leucocratic and mafic dykes cut the garnet-biotite granites (1-2%) and are discussed in Section 2.8.

The petrographic features of the garnet-biotite granites are summarized in Table 2.2, and with the exception of grain size and variable mineral compositions they are petrographically indistinguishable. Briefly the features include euhedral microcline microperthite phenocrysts, euhedral to subhedral normal oscillatory zoned andesine-oligoclase with sodic rims, especially adjacent to K-feldspar where myrmekitic textures are developed, euhedral to subhedral dark brown biotite and equant undulose quartz grains. In extreme cases interstitial orthoclase forms oikocrysts encompassing all the major mineral phases. The formation of granophyric textures (Plate 2.11) or zoning in some microperthites suggests a change in crystallization conditions, possibly during intrusion. The compositional variation of the microperthite from rim to core is presented in Table 2.3.

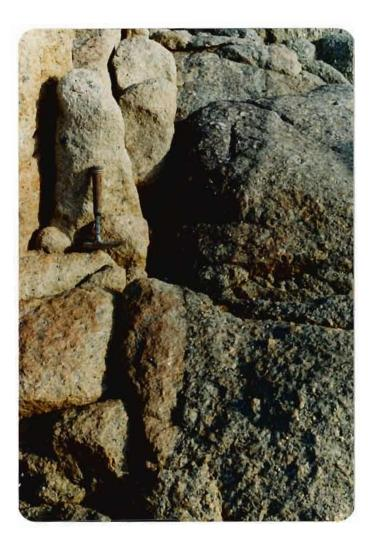
Garnet and cordierite, with biotite, occur as accessory phases in the granite (less than 0.5%) and are found at the margins of igneous xenoliths and as layers and blebs (Plates 2.12a,b; 2.13a,b). Cocker (1977) interprets these garnet-biotite-cordierite layers and bleb associations as early flow concentrations. This study, unlike the study of Cocker, found garnet and cordierite almost always adjacent to the margins of igneous inclusions. Garnet is also commonly found occurring within igneous xenoliths. Field evidence suggests that assimilation has played an essential role in the garnet and cordierite crystallization. The occurrence of anhedral

29

and the second second



Plate 2.11 Granophyric textures in a microperthite from the garnet-biotite granite (#63066).





Plates 2.12(a)(b) Garnet-biotite-cordierite rims to alkali feldspar granite Xenoliths, Boulder Point and Deep Creek, respectively.





- Plate 2.13(a) Garnet-biotite-cordierite accumulation within the garnet-biotite granite, Picnic Rocks.
- Plate 2.13(b) Porphyritic mafic xenolith with a garnet-biotite rim, Picnic Rocks.

Microcline microperthite					Plagioclase exsolution			
	Са	Na	K		Са	Na	K	
edge	0	11	89	edge	1	85	14	
	0	12	88		2	98	0	
	0	14	86		11	89	0	
	0	23	77		3	95	2	
core	0	9	91	core	0	100	0	

Table	2.3	Compositional variation (zoning)
		in microcline microperthite
		(#63066).

garnets enclosed by primary red-brown biotite (Plate 2.12a,b) has been suggested to represent replacement of the garnet at temperatures above the solidus (Cocker, 1977).

The suggested primary mineral paragenetic sequence for the porphyritic garnet-biotite granite is presented in Figure 2.11.

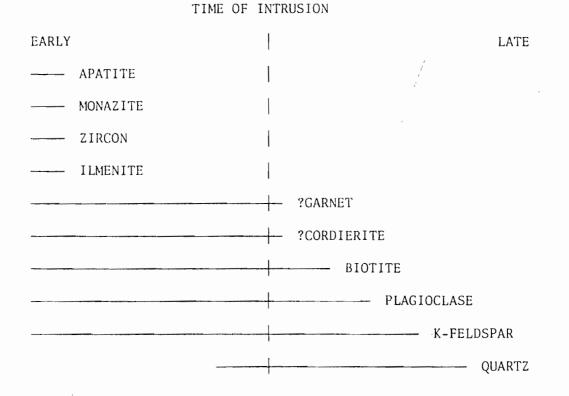


Figure 2.11 Primary mineral paragenesis for garnet-biotitecordierite granites. Modal analyses of the porphyritic garnet-biotite granitoids restrict them to the granite field of Streckiesen (1976) (Figure 2.1). Specimen #63051, is an exception and plots within the granodiorite field.

2.7 ALKALI-FELDSPAR GRANITE

A pink or cream coloured, equigranular, medium grained granite containing approximately 1% muscovite and 2-3% biotite outcrops on the hills 6 km north and south of the Mt William summit. Outcrop is aligned along a regional contact separating hornfelsed Mathinna Beds to the west from the coarsely porphyritic garnet-biotite granite to the east. Outcrop also occurs sporadically among coastal exposures from Boulder Point to Musselroe Point. At Boulder Point contacts with the garnetbiotite porphyrites are near vertical with chilled margins (Plate 2.14), indicating the alkali-feldspar granites were a later intrusive phase. At Mt William, Jennings (1977) described the contact relationships as "enigmatic", field evidence neither confirming a shallow nor a steeply dipping intrusive sheet reportedly characteristic of the alkali-feldspar granite in the Blue Tier Batholith (Groves, 1971).

The petrographic features of the alkali-feldspar granites have been summarized in Table 2.2. They consist of interlocking euhedral-subhedral laths of zoned albite and microperthitic to mesoperthitic interstitial aggregates of microcline with graphic quartz intergrowths. The micas are characteristically free of accessory minerals but remnant pleochroic haloes are present in the brown to pale brown biotites. Medium grained muscovites (lithium-rich), secondary in appearance replace K-feldspar and plagioclase (Plate 2.15).

The primary mineral paragenetic sequence for this rock type is presented in Figure 2.12.



Plate 2.14(a) Chilled margin to the alkali feldspar granite next to a porphyritic garnet-biotite granite, Boulder Point.



Plate 2.14(b) A disturbed chilled margin to the alkali feldspar granite, suggesting a series of intrusive pulses for emplacement. Boulder Point.

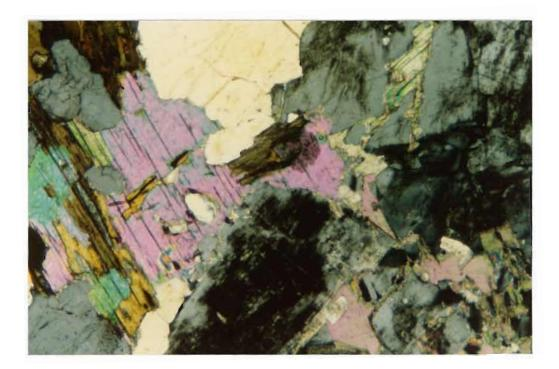


Plate 2.15 Secondary muscovite replacing K-feldspar and plagioclase ($\ \)$, x $\ .$

· · · · · · · · ·

.

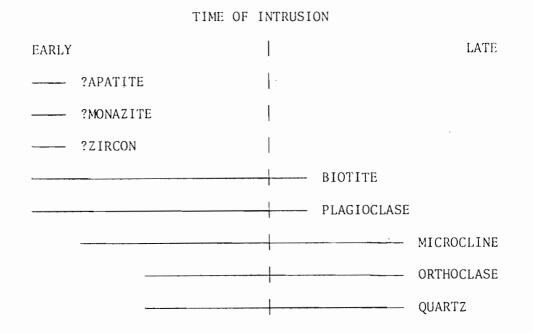


Figure 2.12 Primary mineral paragenesis for the alkalifeldspar granite.

Modal analyses of the alkali-feldspar granitoids (Figure 2.1) classify the rock type as a granite (Streckeisen, 1976), because the sodicrich phases stained red and were point-counted as plagioclase.

2.8 LEUCOCRATIC AND MAFIC INTRUSIVES

2.8.1 Aplite Dykes

Aplitic dykes intrude Mathinna Beds and granites throughout the Ansons Bay Batholith, and at Eddystone Point an aplitic swarm represents the largest concentration of these leucocratic intrusions.

In outcrop, the dykes range in width from 2 cm to 2 m, and appear to cut the mineral foliation at right angles (Figure 2.9). Dykes often bifurcate and rejoin within a few metres, and at Eddystone Point evidence of two stages of aplitic intrusions are suggested by offset and intersecting aplitic dykes (Plate 2.16a,b).

Petrographically the aplite is a granular intergrowth of quartz and feldspar crystals, often with graphic textures, plus biotite and muscovite. The aplites can be separated north and south of Eddystone Point,

based on grain size and biotite geochemistry. The northern aplites have a coarser grain size and lower Mg/Mg+Fe ratio, similar to the host rock which is a coarse porphyritic garnet-biotite granite. Modal analyses classify the aplites as granites according to Streckeisen (1976) (Figure 2.1).

2.8.2 Porphyritic Mafic Aplite Dykes

A porphyritic mafic aplite dyke outcrops at each of three locations: Deep Creek, Boulder Point, and 2 km northwest of Boulder Point.

In outcrop, these mafic dykes are approximately 15 cm wide, have undulating margins, K-feldspars roughly orientated parallel to the margins and a fine grained groundmass in which biotite occurs as books or fine grained aggregates (<2 mm) (Plate 3.17a,b).

The mafic dyke northwest of Boulder Point is affected by shearing which boudinaged and pinched-out the ends of the dyke resulting in biotiteand quartz-rich layers (schlieren).

2.8.3 Pegmatite Dykes

Pegmatitic dykes of quartz and K-feldspar with minor tourmaline, biotite and muscovite, occur frequently throughout the Ansons Bay Pluton cutting across all previous granitic structures and aplite intrusions (Plate 2.18a). Plate 2.18b shows the coarseness of a pegmatitic dyke, exhibiting euhedral K-feldspar phenocrysts in a quartz groundmass.

2.8.4 Microgranite Dykes

Microgranite dykes 3 m wide and of uncertain length outcrop on the foreshore north of Purdons Bay (Fig. 2.3). The microgranite has a uniform grey, fine grained texture interrupted by random subhedral feldspar phenocrysts up to 8 mm long. It is texturally identical to the Musselroe Point Microgranite. The margins of the dyke are undulose and in places bifurcate into the host rock, suggesting intrusion took place



Plate 2.16(a) Bifurcating aplite dyke in the Boulder Point Granodiorite, Boulder Point.



Plate 2.16(b) Offset, intersecting aplite dykes, Eddystone Point.



Plate 2.17(a) Undulating margins of a porphyritic mafic aplite dyke, Boulder Point.

Plate 2.17(b) Porphyritic mafic aplite dyke with subparallel orientated K-feldspar megacrysts. A porphyritic mafic xenolith is also present. Deep Creek.



Plate 2.18(a) Pegmatite dyke cutting biotite schlieren in the Eddystone Point biotite granite, Eddystone Point.



Plate 2.18(b) Coarsely pegmatitic dyke exhibiting euhedral K-feldspar megacrysts, Eddystone Point.

while both were relatively unconsolidated (Plate 2.19a,b).

Petrographically the microgranite has subhedral to euhedral oligoclase, subhedral brown biotite with chloritic alteration, discrete quartz grains with distinct undulose extinction, and interstitial microcline.

Modal analyses of the microgranite (#63082) classify it as a granite, according to Streckeisen (1976) (Figure 2.1).

2.8.5 Dolerite Dykes

North-south oriented doleritic dykes up to 10 km long and 3 m wide intrude the granitoids and Mathinna Beds north of Bayleys Hill (Figure 2.3).

These dykes (Plate 2.20a,b) have previously been described by P. Collins (cited in Jennings, 1977):

"Porphyritic mafic dykes, of variable thickness and with welldefined margins, intrude the Devonian granitic rocks and the Mathinna Beds of northeastern Tasmania. The dykes, which have a macroscopic texture similar to the Jurassic dolerites, consist of subidiomorphic plagioclase phenocrysts in a fine to mediumgrained subophitic groundmass of augite, hornblende and plagioclase. Chloritised biotite, iron oxides, sulphides and apatite are common although minor constitutents, and a little quartz and orthoclase may occur interstitially. The plagioclase is dominantly andesine, and the phenocrysts, which are ubiquitous but not always abundant, are commonly zoned and less than 10 mm in length. Augite is often partially to completely altered to a secondary fibrous amphibole (uralite), and partial sericitisation of the plagioclase is common. The hornblende may be of secondary origin, although this is not obvious."

The dolerité differs from the Tasmanian Jurassic dolerite in three important ways (N. Ortez, pers. comm., 1982): 1) Plagioclase is dominant to ferromagnesium minerals (in Jurassic dolerite the ratio is 50:50).

 Possesses extreme pyroxene (augite) alteration to amphibole and biotite which is not usually found in Jurassic dolerite (uralitization).
 Unusual to have fresh plagioclase in a very weathered and altered groundmass.



Plate 2.19(a) Microgranite dyke with undulose margins, south of Cod Bay.



Plate 2.19(b) A margin of the microgranite dyke and porphyritic biotite-garnet granite. This suggests that both were relatively unconsolidated during the microgranite intrusion. Cod Bay.



Plate 2.20(a) Petrographic features of the Devonian dolerite dykes, Mt William. Plane polarized light, x8 (#63095).



Plate 2.20(b) Devonian dolerite dykes, crossed polarized light, x8. (#63095).

All of these features suggest that the dolerite dykes are probably associated with late-stage crystallization of the Devonian granites (Collins, op. cit.), i.e. they are Devonian dolerites.

2.8.6 Lamprophyre Dyke

A lamprophyre dyke, poorly exposed, outcrops on the foreshore at the southern end of Cod Bay.

In handspecimen the green-black lamprophyre contains dark green prismatic amphibole phenocrysts $3 \text{ m} \times 4 \text{ mm}$, and feldspars up to 4 mmlong with recrystallized edges in a fine grained groundmass.

Petrographically the lamprophyre has euhedral-subhedral hornblende phenocrysts up to 3 mm with khaki and green pleochroism, plagioclase phenocrysts up to 2.5 mm with carbonate reaction rims and skeletal iron oxide crystals less than 0.25 mm, in a groundmass of 0.1-0.2 mm plagioclase laths and carbonate alteration products (Plate 2.21a,b).

The calc-alkaline lamprophyre has been identified as a hornblendeplagioclase spessartite, which has been attributed to hybridization between basic magma and granitic residua or sediments (Rock, 1977).

2.9 INTRUSIVE SUCCESSION

The inferred intrusive succession for the Ansons Bay Batholith is based on field relationships and age determinations for northeast Tasmanian granitoids. Biotite ages for these granitoids suggest that the age decreases from granodiorite, to biotite granite, to garnet-biotite granite, to alkali-feldspar granite.

In the Ansons Bay Batholith the Gardens Pluton Granodiorite has been dated by Cocker (1982) at 383 Ma and intrudes and contact metamorphoses the low grade, regionally metamorphosed Ordovician to Lower Devonian Mathinna Beds. The Boulder Point Granodiorite has not been dated and has no visible field contacts, but is assumed to be of comparable age to

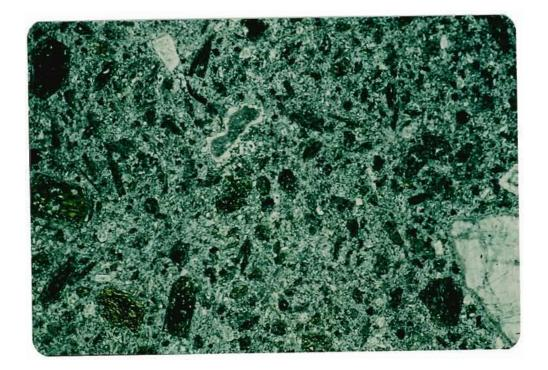


Plate 2.21(a) Petrographic features of the lamprophyre dyke, Cod Bay. Plane polarized light, x9 (#63096).

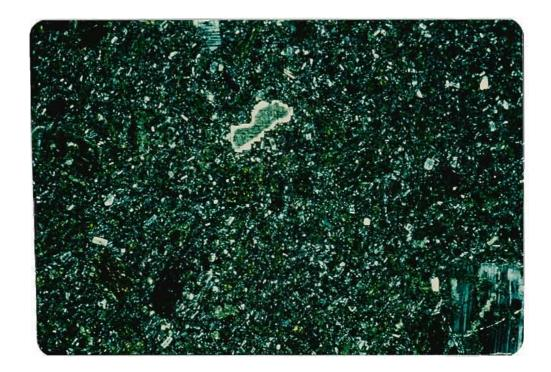


Plate 2.21(b) Lamprophyre dyke, crossed polarized light, x9 (#63096).

the rest of the granodiorites of northeastern Tasmania.

The biotite granites occur as two separate granitoids, the Eddystone Point and the Ansons Bay biotite granites. The Eddystone Point biotite granite has intrusive contacts with the Mathinna Beds but contacts with other granitoids are obscured by Quaternary sands and gravels. The Ansons Bay biotite granite, on the other hand, has a poorly exposed granitoid contact, and extreme weathering prevents relative age determinations. The biotite granites intrusive sequence cannot be interpreted from field contacts and must be assumed to succeed the granodiorite based on regional biotite dates for the northeastern Tasmanian granitoids.

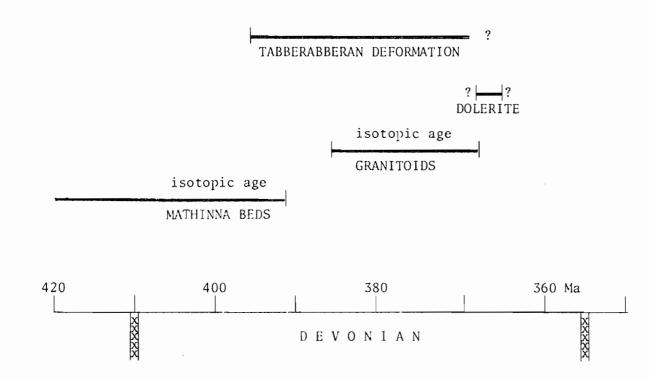
Garnet-biotite granites of the Ansons Bay Batholith have been dated at 375 Ma and are therefore younger than the granodiorites and possibly younger than the biotite granites. Field relationships indicate that the garnet-biotite granites are older than the alkalifeldspar granites which have chilled margins along their contacts. The garnet-biotite granites are however syngenetic with the microgranites for the reasons outlined previously. The metasomatised alkali feldspars therefore represent the final stages of granitoid intrusions, possibly 370 Ma (Cocker, 1982).

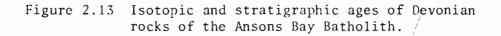
A series of dyke intrusions followed the major granitoids. The first of these was syngenetic to post solidification, and were the porphyritic aplite dykes which exhibit straight, undulose and broken margins. This set of dykes was probably associated with the remobilization of a volatile magma as shown in Figure 2.10. Microgranite dykes exhibit similar features. The fine grained aplite dykes lack undulose and broken margins suggesting intrusion into solidified magmas. Pegmatite dykes cut all the major granitoids, xenoliths and aplites indicating that they occurred late in the intrusive sequence.

Dolerite dykes up to 10 km long occur within the northern section of the Ansons Bay Batholith, intersecting Mathinna Beds, garnetbiotite granite and alkali-feldspar granite. They are interpreted to be Devonian dolerites and may have intruded along faults produced during the Tabberabberan Orogeny. If this is the case then the Tabberabberan Orogeny in northeastern Tasmania must have undergone several deformation phases to, firstly, produce the regional-scale folding in the Mathinna Beds after the deposition of the arenite-lutite sediments, and, finally, to produce the necessary fault systems(?) associated with the dolerite intrusions. The possible age of the Tabberabberan Orogeny therefore ranged from 401 ± 7 Ma (metamorphosed Mathinna Beds; Cocker, 1982) to less than 370 Ma (age of the alkali-feldspar granites in northeastern Tasmanian). Age determinations for the dolerite should provide a lower age limit for the Tabberabberan Orogeny due to little or no postintrusive deformation within the granitoids of the Ansons Bay Batholith after this event.

The occurrence of a single lamprophyric dyke is attributed to hybridization between basic magma and granitic residue or sediments, and is associated with late-stage doleritic intrusions, i.e. the final stages of the Tabberabberan Orogeny. An isotopic and stratigraphic summary of the Devonian rocks of the Ansons Bay Batholith is presented in Figure 2.13.

+0





Chapter 3

GEOLOGY, PETROGRAPHY AND GEOCHEMISTRY OF THE AGMATIC MIGMATITE CONTACT

3.1 INTRODUCTION

An agmatic (brecciated) contact between hornfels Mathinna Beds and garnet-biotite granite occurs at a coastal exposure 3.5 km southwest of Eddystone Point (Figure 3.1). The Mathinna Beds may represent a large raft of country rock within the garnet-biotite granite. This interpretation is supported by the occurrence of Mathinna rafts 3 km northwest of Eddystone Point, and the different orientation of the country rock at the western contact near Icena Creek (220° W 83° , 020° E 78° respectively). The variation in dip and dip direction may however result from pressures exerted by the magma on intrusion of the country rock. Evidence for forceful intrusion can be found in the asymmetrically open folded layers in the metamorphosed country rock adjacent to the contact (Plate 3.1).

3.2 STRUCTURE OF THE AGMATIC MIGMATITE CONTACT

The term *migmatite* was coined by Sederholm (1907; cited in Sederholm, 1967) and is used in the sense defined by Mehnert (1968):

"A migmatite is a megascopically composite rock consisting of two or more petrographically different parts, one of which is the country rock, generally in a more or less metamorphic stage, the other is of pegmatitic, aplitic, granitic, or general plutonic appearance."

The migmatite described exhibits only contact features and does not pass through all stages of migmatite formation associated with true migmatitic terrains.

The trend of the migmatite contact is approximately northeast, truncating the bedding at 90[°]. This is the case for the Bridport Migmatite Contact (Skrezeczynski, 1971) and is a feature which Marshall (1969) considers to be joint controlled. The irregular edge of the contact gives

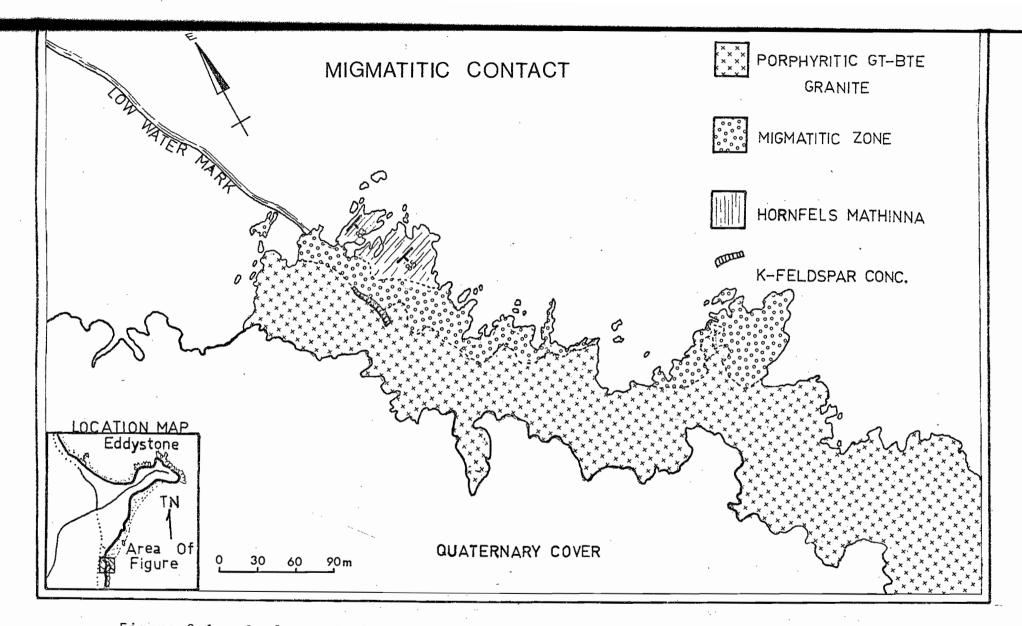


Figure 3.1 Geology of the agmatic migmatite contact, south of Eddystone Point.



Plate 3.1 Asymmetrically open folded layers in the metamorphosed Mathinna Beds adjacent to the agmatic migmatite, south of Eddystone Point.



Plate 3.2 Garnet-biotite granite, neosome (newly formed rock) and paleosome (unaltered or slightly modified country rock) at the agmatic migmatite, south of Eddystone Point.

the impression of torn bedding, and the dip of the contact approximates the vertical plane, features which are all consistent with the Bridport Migmatite Contact.

The agmatic contact migmatite between the garnet-biotite granite and the hornfels Mathinna Beds south of Eddystone Point consists of a brecciated transition zone 10-30 m wide and 300 m long. This zone exhibits agmatic (breccia), diklyonitic (veinlet networks), schollen (raft) and phlebitic (vein) structures.

The garnet-biotite granite can be distinguished from the darker neosome (the newly formed rock portion) of the transitional zone which in turn can be distinguished from the paleosome and hornfelsed country rock (the unaltered or only slightly modified country rock) (Plate 3.2).

Three types of xenoliths in the garnet-biotite granite have been identified. The country rock paleosome is the most common. Other xenoliths are a mafic-porphyritic xenolith, and a single occurrence of an equigranular biotite xenolith (63117). The paleosomes range in size from micro-inclusions to inclusions a few metres in diameter, and vary in outline from angular blocky xenoliths in the granite to well rounded prolate spheroids in the neosome (Plate 3.3a,b). The angularity of the paleosomes in the granite appear to have resulted from assimilation along jointing and weaker more fissile layers. In the apparently more mobile neosome, the paleosomes are well rounded suggesting magmatic corrosion and abrasion. The rounding can also be interpreted as the co-existing of two different viscosity melts similar to the microgranite/granite contact at Musselroe Point. This may explain near identical paleosome and neosome occurrences in some cases (Plate 3.4).

A characteristic feature of the paleosome is the presence of relict bedding laminations. Some laminations are curved suggesting left lateral shearing across the contact (Plate 3.4), parallel with the K-feldspar mineral foliation of the granite. Another feature of the country rock 53



Plate 3.3(a) Angular blocky paleosome in the garnet-biotite granite next to the agmatic migmatite, south of Eddystone Point.



Plate 3.3(b) Rounded prolate spheroid paleosomes in the neosome of the agmatic migmatite, south of Eddystone Point.

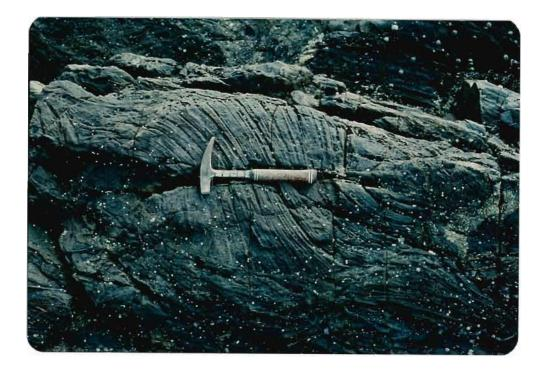


Plate 3.4 Almost compositionally identical paleosome and neosome from the agmatic migmatite, south of Eddystone Point. Note the left laterally curved laminations of the paleosome.

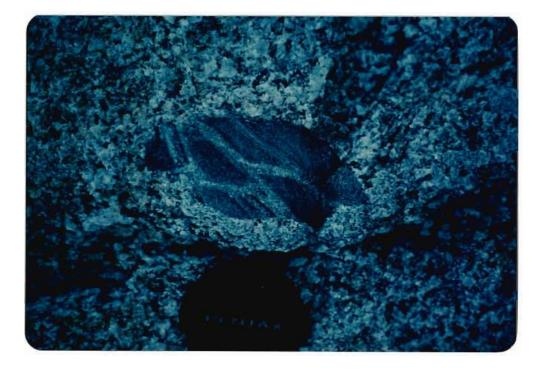


Plate 3.5(a) Diklyonitic (veinlet network) structure within a paleosome from the agmatic migmatite, south of Eddystone Point.



Plate 3.5(b) A paleosome with continued pervasive dissection and assimilation, south of Eddystone Point.



Plate 3.5(c) Paleosomes sitting in the neosome, a result of the dissection and assimilation of the country rock. Agmatic migmatite, south of Eddystone Point. xenoliths is their occurrence as aggregates within the granite. This suggests pervasive dissection and assimilation of the paleosome by the granite melt to form diklyonitic, schollen and phlebitic structures. This is well illustrated by the three plates 3.5a,b,c.

Granitic veining and pods within the highly deformed Mathinna Beds intrude along steeply dipping bedding planes, joints and cracks, "peeling off" and assimilating the country rocks (Plate 3.6a,b).

The Mathinna Beds are fine grained, biotite-muscovite hornfels with compositional banding (bedding) due to the differential metamorphism of the arenite and lutite beds. The neosome, which is predominantly quartzitic, however, varies in composition to granitic material (Plate 3.7). The neosome is therefore postulated to have been derived from the country rock by isochemical re-equilibration with granitic magma.

3.3 PETROGRAPHY OF THE AGMATIC MIGMATITE CONTACT

Thin section descriptions of the garnet-biotite granite are given in Section 2.6, and Table 2.2. Its features (63057) include cuhedral microcline microperthite phenocrysts up to 30 mm with granophyric intergrowths defining a previous crystal outline. Euhedral-subhedral oscillatory zoned andesine-oligoclase crystals (core An_{37} -rim An_{20}) exhibit sodic rims, especially adjacent to K-feldspar crystals where myrmekitic textures are common. Biotite occurs as euhedral-subhedral dark brown laths with inclusions of apatite, monazite, zircon plus ilmenite, and quartz is equant and undulose with biotite inclusions. Orthoclase occurs interstitially generally with inclusions of most of the major phases.

The granophyric intergrowths of vermicular quartz and microcline (Plate 5.8) defining previous crystal outlines have been interpreted to represent changing conditions of crystallization, possibly intrusion. Should this be the case, it implies that the major minerals present as crystals in the melt during intrusion and formation of the agmatic

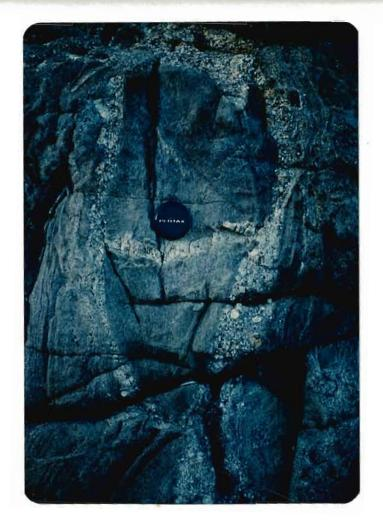


Plate 3.6(a) Porphyritic granite intruding along bedding planes, joints and cracks of the Mathinna Beds. Agmatic migmatite, south of Eddystone Point.

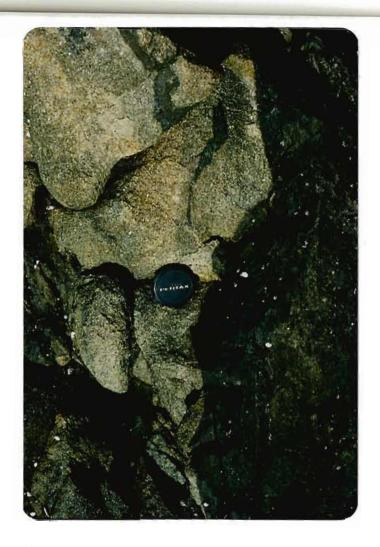


Plate 3.6(b) Granitic pod intruding the Mathinna Beds, agmatic migmatite, south of Eddystone Point.



Plate 3.7 Variation of the neosome from quartzite to granite. Agmatic migmatite contact, south of Eddystone Point.

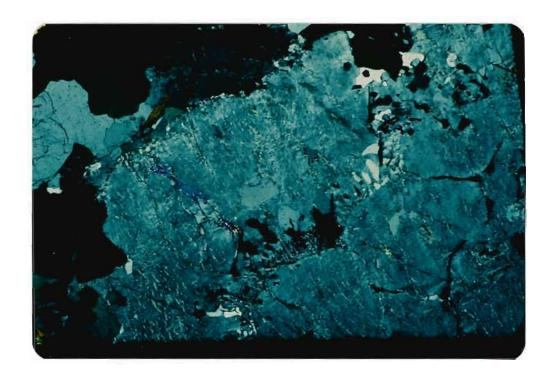


Plate 3.8 A section of a granophyric intergrowth between vermicular quartz and microperthite outlining a previous crystal outline (#63057, crossed polars, x 15).

59

migmatite were biotite, plagioclase, K-feldspar and quartz.

Thin section studies suggest the weak foliation of the garnetbiotite granite is due to primary flow rather than a later cataclastic deformation after crystallization (i.e. there is no evidence of deformation of any of the mineral phases).

The modal analysis of the garnet-biotite granite (63057, Appendix 1, Figure 2.1) is consistent with other modal analyses for the garnet-biotite granites. A granitic pod (63058) from within the deformed country rock however plots (Figure 2.1) very close to the alkali syenite field of Streckeisen (1967).

The granitic pod (63058) is a fine grained massive leucocratic rock with minor fine grained biotite laths. Petrographically (Plate 3.9) it is composed of K-feldspar (orthoclase) with granophyric quartz, giving the rock a mottled texture. Plagioclase is absent, and biotite laths are chloritized. Some of the secondary chlorite has a sagenitic texture caused by the exsolution of a titanium-rich phase (rutile) during the alteration of biotite to chlorite. This texture is only observed in the secondary chlorites of the granitic pod, paleosome and neosome, but not in the granite, suggesting that the biotite in the migmatite is more titanium-rich.

The Mathinna paleosomes in the migmatite exhibit various stages of digestion. They range from unaltered contact hornfels with sharp contacts with the neosome, to partially assimilated paleosomes with complex relationships with the neosome.

The contact metamorphosed hornfels contains spots (5 mm) which are grey and ovoid in contrast to the dark grey groundmass. Petrographically (63098, Plate 3.10) the spots are ovoid or elongate aggregates of fresh xenoblastic and poikioblastic cordierite with fine biotite and iron ore rims, similar to the Bridport example (Skrezeczynski, 1971). The groundmass consists of very fine grained (average 0.05 mm) quartz, sericite, chlorite and iron ore. The biotite and iron ore flakes (average 0.1 mm) that are

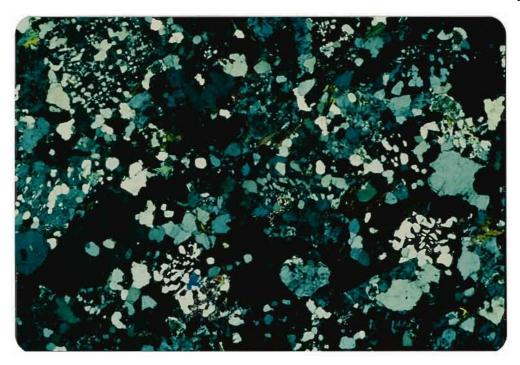


Plate 3.9 Graphic quartz-orthoclase intergrowths from the granitic pod (#63058, crossed polars, x 9).



Plate 3.10 Ovoid poikioblastic cordierite in the spotted hornfels of the contact metamorphosed Mathinna Beds. (#63098, plane polars, x10).

aligned around the rim of the poikioblasts are due to crystalloblastic forces pushing aside the components of the groundmass or partly enclosing them (Augustithis, 1973).

It has been suggested by Skrezcezynski (1971) that the banding between spotted and unspotted hornfels, observed in the country rocks and paleosomes, resulted from lutite and arenite alternations in the original sediment. Skrezeczynski (1971) and Van Moort (1966) found cordierite preferentially developed in the pelite because of the higher alumina, iron oxide and MgO content relative to the psammitic sediments (63097, Plate 3.11).

In the coarser quartz-rich layers (Plate 3.12), biotite is the first metamorphic mineral to form, producing a typical granoblastic texture with quartz. The biotite laths are preferentially aligned parallel to bedding, and are suggested to have resulted from a reaction between chlorite, muscovite and iron oxide originally present in the sediment (Tilley, 1924; Harker, 1939).

As expected, paleosomes in the migmatite show relict country rock structures of psammitic and pelitic alternations. Characteristic psammitic paleosomes (63104) only vary in their sericite and and muscovite contents when compared to the contact metamorphosed country rock. Their quartzsericite-biotite-muscovite mineral assemblage lacks cordierite and chlorite, characteristic of the psammitic-rich country rocks.

Petrographically the psammitic paleosomes (63104) exhibit granoblastic to lepidoblastic hornfelsic textures. Quartz (average 0.2 mm) is the most abundant mineral, and forms a mosaic of grains with deeply sutured boundaries. It exhibits weak undulose extinction and often contains inclusions of iron ore and biotite. The brown biotite flakes (average 0.1 mm) are strongly aligned and are free of inclusions. Interstitial sericite and muscovite form the matrix between the biotite and quartz grains.



Plate 3.11 Preferential development of spotted cordierite in pelitic layers relative to psammitic layers of the Mathinna Beds at the contact migmatite. (#63097, crossed polars, x6)

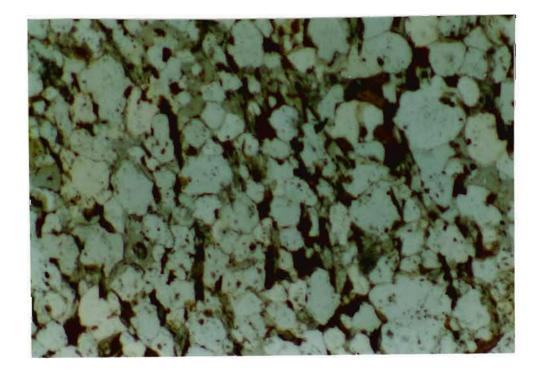


Plate 3.12 A typical granoblastic texture in the psammite layers of the Mathinna Beds (#63100, plane polars, x32)

The pelitic paleosomes are semi-schistose, consisting predominantly of muscovite-sericite overgrowths with inclusions of relict quartz and biotite. Irregular cordierite grains up to 3 mm also occur.

The neosome varies in composition from quartzitic to granitic and is postulated to have been derived from the country rock by partial assimilation with the granite. Petrographically the neosome is a fine to medium grained rock with a flow structure evident through the development of granoblastic dykelets of quartz outlined by biotite (chloritized) in a matrix of finer quartz and K-feldspar (average grain size 2 mm). The groundmass consists of biotite, sericite and muscovite less than 0.5 mm.

Cordierite is reasonably abundant in most specimens and occurs as square or prismatic porphyroblasts up to 2 mm in length. Cordierite ranges from fresh to highly altered muscovite and sericite. Andalusite has not been recognized.

In summary, the major feature of the mineral assemblages across the migmatite contact is their dependence on the original composition of the country rock. The psammite mineral assemblage, for example, has chlorite gradually replaced by biotite with increasing metamorphic grade, whereas the pelite mineral assemblage remains relatively constant, varying only in the proportions of biotite and cordierite.

The neosome, interpreted to be derived from the country rocks by assimilation, is not unlike the pelitic layers, differing in the addition of K-feldspar which becomes a major constituent closer to the granite.

64

3.4 P-T CONDITIONS OF FORMATION OF THE AGMATIC MIGMATITE CONTACT

The equilibrium mineral assemblages in the contact hornfels are a lower pressure equivalent of the K-feldspar-cordierite-hornfels facies of Winkler (1965). Winkler, however, has orthoamphibole and orthopyroxene subfacies which are absent from these assemblages

Schreyer & Yoder (1961; cited in Seifert, 1969) in discussing the stability field of cordierite in progressively metamorphosed pelitic rocks suggest the following equation for the derivation of cordierite:

 $(Mg,Fe)_{5}A1(A1Si_{3}O_{10})(OH)_{8} + KA1_{2}(A1Si_{3}O_{10})(OH)_{2} + SiO_{2} \neq$ (hlorite muscovite quartz) $(Mg,Fe)_{2}A1_{4}Si_{5}O_{18} + K(Mg,Fe)_{3}(A1Si_{3}O_{10})(OH)_{2} + 4H_{2}O$ (ordierite) biotite water

Acicular inclusions of rutile are visible under high magnification within some brown biotites suggesting that the biotites are titanium-rich phlogopites. Assuming that phlogopite is an important mineral phase, the equilibrium temperatures associated with the reaction

KAl₃Si₃O₁₀(OH)₂ + Mg₅Al₂Si₃O₁₀(OH)₈ + 2SiO₂ ≠ muscovite clinochlore quartz KMg₃AlSi₃O₁₀(OH)₂ + Mg₂Al₄Si₅O₁₈ + 4H₂O phlogopite cordierite water

in the pure system $K_2O-MgO-Al_2O_3-SiO_2-H_2O$ range from 495 ± $10^{\circ}C$ at 1 kb P_{H_2O} to 635 ± $10^{\circ}C$ at 6 kb (Seifert, 1969), suggesting an epizonal intrusion of the country rock by the garnet-biotite granite.

The absence of aluminosilicates such as andalusite from the neosome mineral assemblage of quartz-biotite-muscovite-chlorite-cordierite-K-feldspar is explained by the reaction (Harker, 1939):

 $\begin{array}{rcl} 2K_2A1Si_3O_8 \ + \ A1_2SiO_5 \ + \ 2H_2O \ \swarrow \ K_2A1_4 \left(Si_6A1_2O_{20}\right) \ + \ SiO_2 \\ \\ potash \\ feldspar \end{array} \qquad and alusite \qquad muscovite \qquad quartz \end{array}$

This reaction suggests that if excess muscovite and quartz occurs then the assemblage aluminosilicate and K-feldspar is unstable and does not coexist.

An AKF diagram (after Eskola, 1939) has been used to show the correlation between mineralogical and chemical compositions in assemblages with excess SiO_2 and Al_2O_3 , where

$$A' = (A1_2O_3) - (CaO + Na_2O + K_2O)$$

 $K = K_2O$
 $F = (MgO) + (FeO) + (MnO)$
and $A' + K + F = 100$.

In Figure 3.2, tie lines have been drawn between the plotted position of minerals normally co-existing in the rocks. The area of each subtriangle represents a range of chemical compositions which have the same mineral paragenesis under K-feldspar-cordierite-hornfels facies conditions. Although two distinct fields of assemblages are plotted, in actual fact the presence of Na allows the co-existence of muscovite-biotite and K-feldspar-cordierite over a wider P-T field (D.J. Ellis, pers. comm., 1982). The reaction (Winkler, 1965)

> 6 muscovite + 1 biotite + 15 quartz 3 cordierite + 8 K-feldspar + 8 H₂O

has the following equilibrium temperatures and related pressures.

 \pm 10°C at P_{H2O} = 500 bars \pm 10°C at P_{H2O} = 1000 bars \pm 10°C at P_{H2O} = 2000 bars \pm 10°C at P_{H2O} = 4000 bars.

The absence of aluminosilicates (andalusite, sillimanite) suggests low pressures, between 500 and 1000 bars and hence a maximum temperature in the order of 600° C was reached adjacent to the contact, indicating that an epizonal intrusion of the country rock by the garnet-biotite granite has taken place.

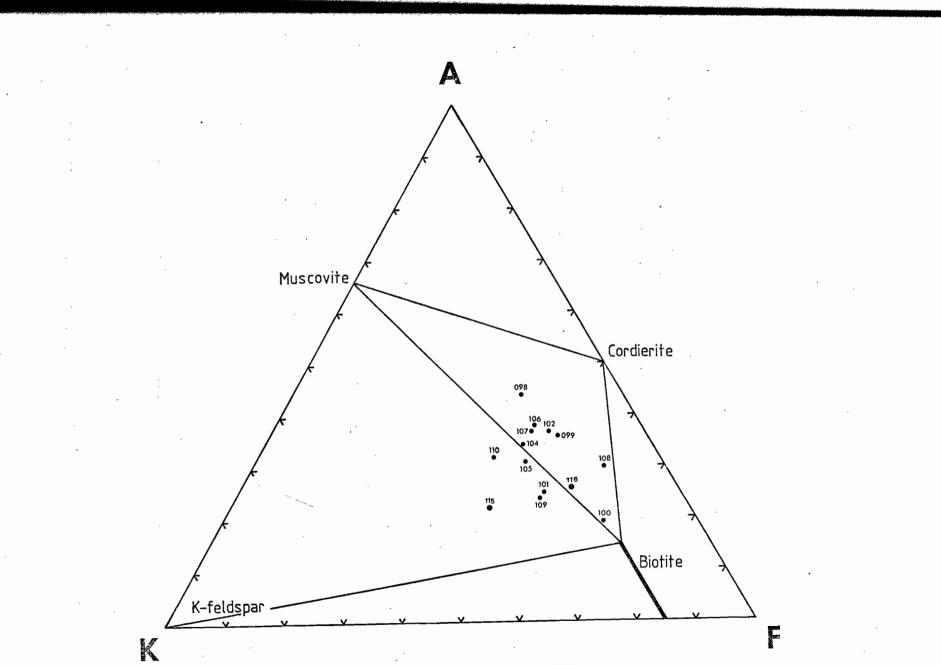


Figure 3.2 AKF ternary diagram (after Eskola, 1939) for the K-feldsparcordierite-hornfels facies of the agmatic migmatite.

•

3.5.1 Introduction

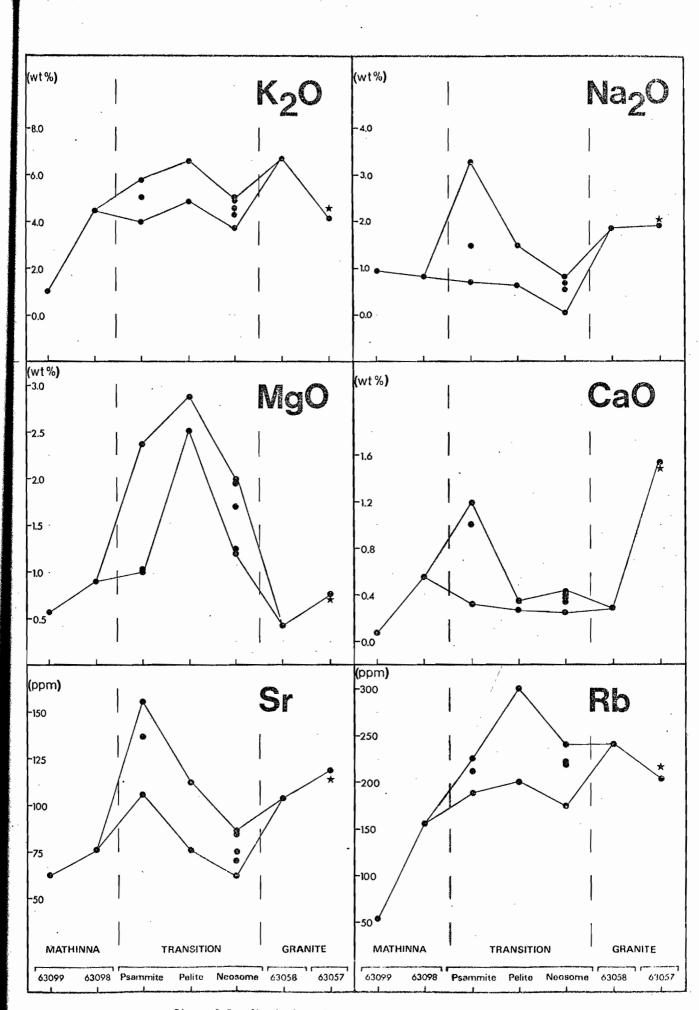
The main aim of this study was to evaluate the chemical variations across the agmatic migmatite contact between country rock and garnet-biotite granite. Sampling followed the techniques outlined in Chapter 1.4. X-ray fluorescence analyses of ten major oxides and eight trace elements were determined for each of the geochemical samples collected and the results have been tabulated in Appendix 2.

3.5.2 Chemical Variation of the Contact Migmatite

A graphical representation of some of the major oxide and trace element variations across the contact migmatite are presented in Figure 3.3. Sample 63099 is an unmetamorphosed arenite, from west of Mt William, and is used for a comparison against the spotted hornfels country rock (63098) adjacent to the migmatite. The transition zone (Figure 3.3) consists of psammite and pelite xenoliths of the paleosome, plus samples taken from the neosome. Sample 63058 is a granitic pod from the transition zone and sample 63059 represents the garnet-biotite granite adjacent to the contact. The asterisk denotes a garnet-biotite granite (63054), 2 km south of the contact at Bayleys Rock, and is used as a comparison for sample 63057.

3.5.3 Discussion of Results

The observed chemical variation across the contact migmatite correlates well with the described petrographic changes. The increasing K_20 , MgO content from the unmetamorphosed country rock to the paleosomes (psammite and pelite) can be correlated with increasing biotite and muscovite mineralogy. As the biotite content decreases, however, toward the granite the MgO value is observed to decline. The formation of K-feldspar, accounts for the continued increase in potassium, attained in the granitic pod, before it decreases slightly in the garnet-biotite granite.



Start Charles

and the second second

Figure 3.3 Chemical variation across the agmatic migmatite.

The Na_2^{0} , CaO values for the contact migmatite are remarkably uniform, from the country rock to the neosome. A single exception is a psammite specimen (63103) which exhibits plagioclase (sodic) porphyroblasts thereby accounting for the anomalous rise in the psammite. The Na_2O content increases from the neosome to the granitic pod, possibly because of the increased substitution of sodium in K-feldspar, becoming constant in the garnet-biotite granites. The CaO content in the rocks, unlike the Na_2O value, does not increase until the garnet-biotite granite where plagioclase becomes a stable mineral phase.

Both rubidium and strontium correlate with the occurrence of potassium and calcium respectively, possibly substituting in the same mineral phases because of similar ionic radii and valency states of these pairs of elements.

3.6 SUMMARY OF THE AGMATIC MIGMATITE CONTACT

The formation of the agmatic contact migmatite, south of Eddystone Point, occurred by an intrusion of a garnet-biotite granite into the Mathinna Beds under P-T conditions of 600° C and 1000 bars.

Field relationships, petrography and geochemical evidence suggest that assimilation of the country rocks has occurred, however at this level contamination of the garnet-biotite granite appears to be restricted to within a few metres of the contact (samples 63057, 63054).

Chapter 4

GEOLOGY, PETROGRAPHY AND GEOCHEMISTRY OF THE GRANITOID XENOLITHS

4.1 INTRODUCTION

The frequent occurrence of xenoliths is a characteristic feature of the Ansons Bay Batholith. The xenoliths have been classified into sedimentary and igneous types, the latter group being subdvided into three further subgroups:

1. Sedimentary (Mathinna Bed) xenoliths

2. Igneous xenoliths

(i) granodiorite mafic xenoliths

(ii) garnet-biotite granite mafic xenoliths

(iii) garnet-biotite granite aplitic xenoliths.

The sedimentary (Mathinna Bed) xenoliths are all but restricted to the migmatite contact of the Ansons Bay Batholith (Chapter 3). Specimens 63114 and 63118, however, are exceptions. Both are K-feldspar rich xenoliths whose mineral paragenesis is consistent with the K-feldspar-cordieritehornfels facies (Section 3.4).

This chapter is concerned with the igneous xenoliths, which form the bulk of the xenolith population within the batholith. /

4.2 MAFIC XENOLITHS FROM THE GRANODIORITE

4.2.1 Geology and Petrography of the Mafic Xenoliths

Mafic xenoliths were collected from the porphyritic Boulder Point Granodiorite (Figure 2.5). Extreme weathering and poor exposure prevented sampling of xenoliths from the Gardens Pluton Granodiorite.

The xenoliths are typically mesocratic to melanocratic, ranging in size from microinclusions to inclusions up to 30 cm, and possessing sharp, well defined boundaries with the granodiorite. They are fine grained (<1 mm)



Plate 4.1(a) Petrographic boundary between a hornblendebiotite-plagioclase mafic xenolith and the host granodiorite (#63020, plane polarized light, x20).



Plate 4.1(b) #63020, crossed polarized light, x20.

and dioritic in composition. In hand specimen their texture is granoblastic, commonly containing plagioclase megacrysts (<5 mm).

Most of the mafic xenoliths are rich in biotite relative to hornblende, although one xenolith (63120) is distinctly hornblende-rich, and another (63127) contains biotite as the only mafic phase. Modal compositions of the dioritic xenoliths (63119-63129) contain 45-55% plagioclase (An_{35-45}) , 20-40% biotite, 5-35% hornblende, 5-10% interstitial quartz plus accessory apatite (<2%) and tourmaline. The xenoliths have a sub-parallel orientation of plagioclase laths, hornblende crystals and biotite flakes and their orientation is disrupted by plagioclase megacrysts (<7 mm). This suggests the xenoliths have had a tectonically induced foliation, parallel to their long axis.

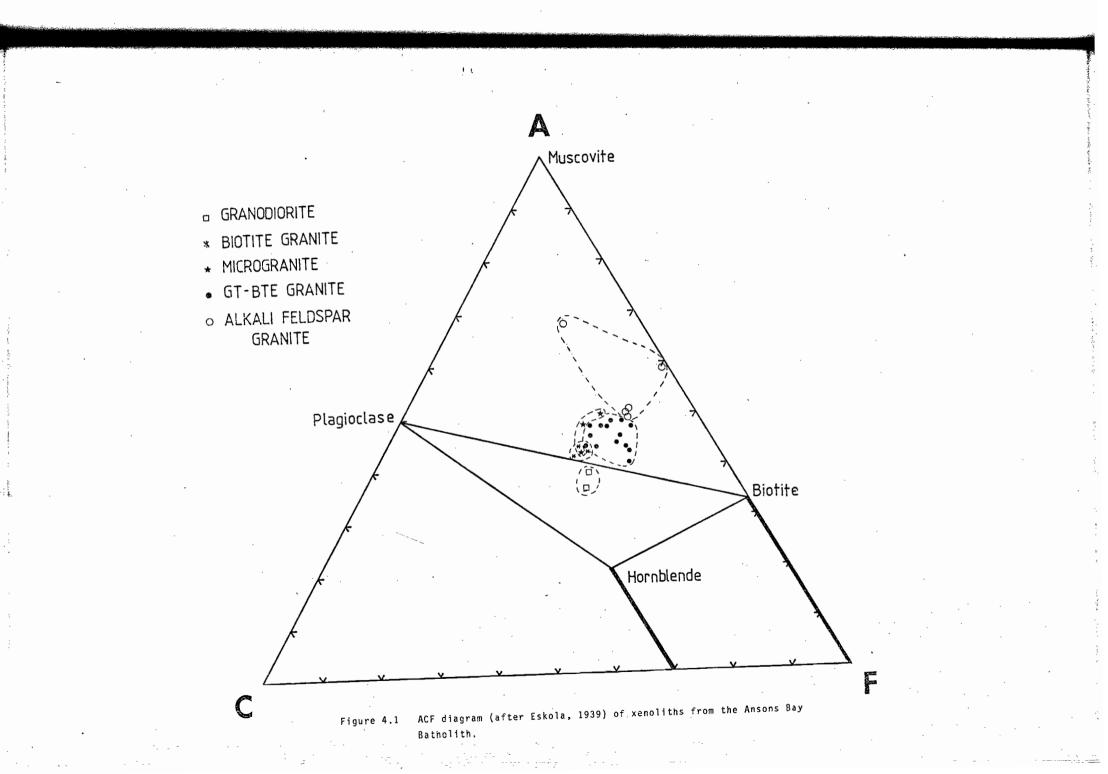
Biotite commonly occurs as small euhedral-subhedral columnar flakes (2 mm) with inclusions of zircon, apatite, quartz and monazite. Hornblende occurs as individual subhedral-anhedral crystals (average 2 mm) or as intergrown aggregates (<4 mm).

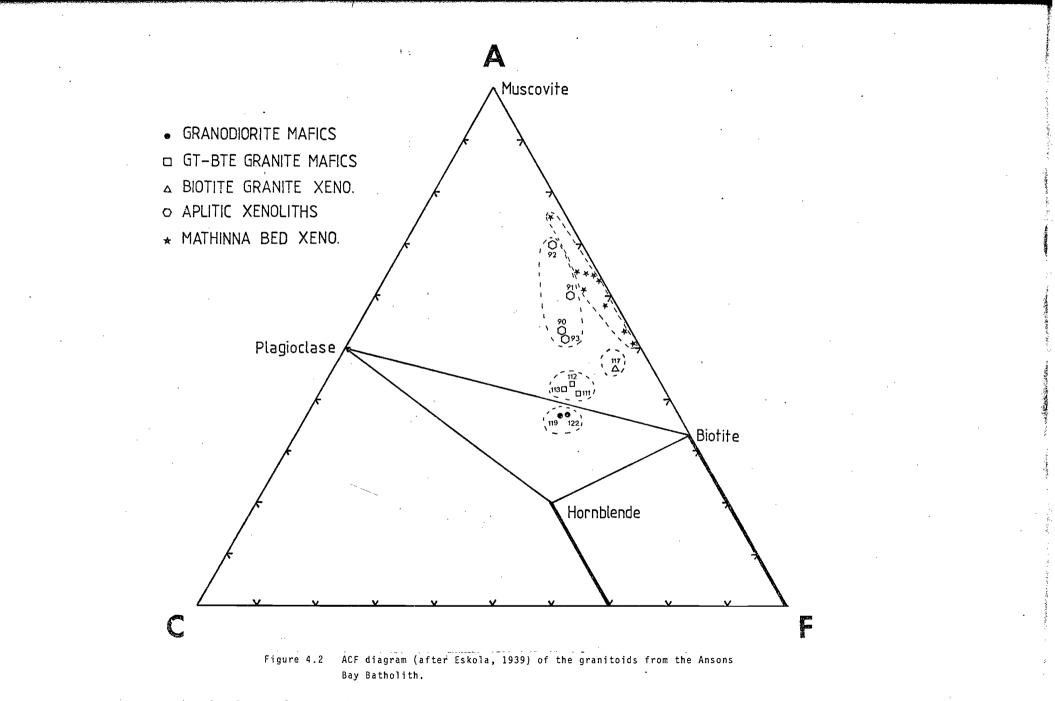
In thin section the boundaries between the xenoliths and the granodiorite are usually irregular, but well outlined by a distinct variation in grain size and composition (Plate 4.1).

4.2.2 Facies Diagrams for the Granodiorite Mafic Xenoliths

The equilibrium mineral assemblages for the mafic xenoliths are typical of the hornblende-hornfels facies of Turner (1968). An ACF diagram (Figure 4.1, after Eskola, 1939) has been used to show the correlation between mineralogical and chemical compositions with excess SiO_2 and K_2O deficiency.

The valency state of iron was not determined by the analytical techniques used and therefore in calculating ACF diagrams iron was considered as Fe^{2+} and added to the F component (Fe^{3+} only occurs as a minor substitute among the mineral phases present).





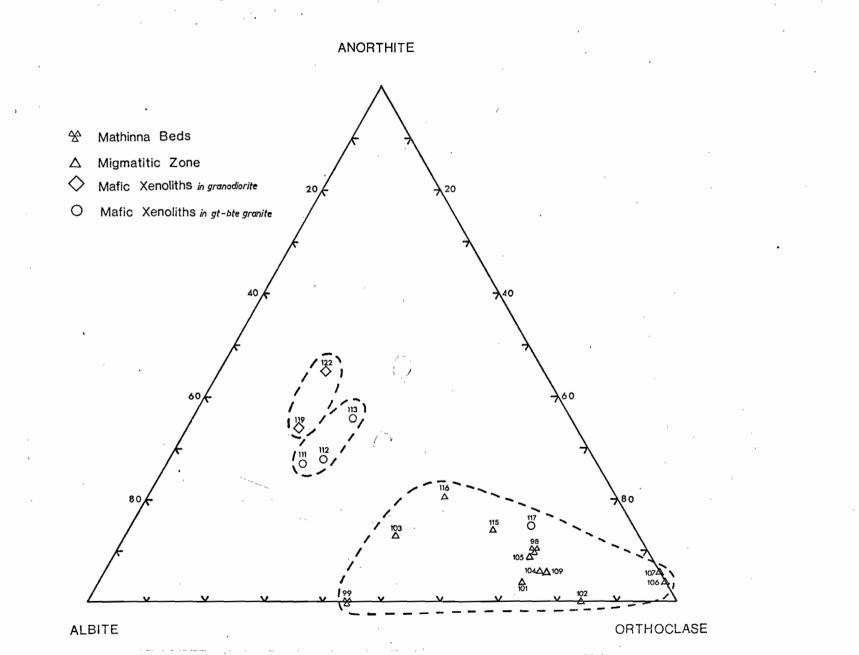


Figure 4.3 An-Ab-Or ternary diagram of xenoliths from the Ansons Bay Batholith.

For sediments (Mathinna Beds), however, an Fe^{3+} to Fe^{2+} ratio of 3:1 was used in calculating those values plotted on the ACF diagram (Parker, 1967).

In the triangular facies diagram (Figure 4.1), tie lines have been drawn between the plotted position of the minerals normally coexisting in the rock (plagioclase-biotite-hornblende). The mafic xenoliths plot within the subtriangle corresponding to their petrographically observed assemblages. Because they plot beneath the plagioclase-biotite tie line which separates I- and S-type granites (White & Chappell, 1977) this implies that the mafic xenoliths are cognate (i.e. they are genetically related to the host granodiorite which plots in an identical position, compare Figures 4.1 and 4.2). It is also apparent from the ACF diagram (Figure 4.1) that the granodiorite mafic xenoliths are unrelated to the country rock (Mathinna Beds) xenoliths which plot separately.

In conclusion, the textural evidence, and the ACF diagrams suggest that the mafic xenoliths have a cognate origin.

4.3 MAFIC XENOLITHS FROM THE GARNET-BIOTITE GRANITE

4.3.1 Geology and Petrography of the Mafic Xenoliths

Porphyritic mafic xenoliths occur throughout the garnet-biotite granites of the Ansons Bay Batholith.

These mesocratic porphyritic xenoliths range in size from a few centimetres to 1.5 m in length. They are well rounded with low sphericity, commonly having their long axis aligned parallel to the preferred mineral foliation of the granite. The xenoliths have sharp contacts with the granite and are almost always outlined by garnet-biotite-(cordierite) rims.

In hand specimen (63111-63113; modal analyses of stained slabs where plagioclase stains red, K-feldspar stains yellow, and the remaining minerals are unaffected) point counting indicates the phenocrysts are composed of 10% K-feldspar (<40 mm), 10% plagioclase (<10 mm), and 20% quartz (<8 mm) megacrysts in a fine grained groundmass. Biotite aggregates (<4 mm) also occur within the groundmass (<1 mm) which is composed of biotite, quartz, plagioclase and minor K-feldspar intergrowths. A complete modal analysis is presented in Appendix 1.

The subhedral K-feldspar megacrysts are surrounded by foliated biotite flakes. The K-feldspar megacrysts contain plagioclase and biotite inclusions in a zonal arrangement which mimics the crystal outlines.

The subhedral plagioclase and quartz megacrysts are smaller and more numerous, with no preferred orientation. They also have a distinct biotite foliation around their margins.

An occasional ruby coloured rhombic dodecahedral (<10 mm) euhedral garnet occurs within the mafic xenoliths. Most garnets however, are seen as fragments (1 mm) forming 10 mm aggregates within the xenoliths.

The biotite-garnet (cordierite ?) rims that surround the mafic xenoliths vary in mineralogy from biotite (cordierite ?) to garnet-biotite (cordierite ?). The rims commonly trail off to form biotite schlieren aligned parallel to the K-feldspar mineral foliation of the granite. This suggests that the garnet-biotite (cordierite) rims formed prior to solidification of the granite and were not a subsolidus phenomenon.

Biotite-garnet (cordierite ?) aggregates also occur separately (Plate 2.10b) and are interpreted to be disaggregated rims of mafic xenoliths.

Petrographically the groundmass of the mafic xenoliths exhibit a sieve texture composed of poikiolitic quartz and K-feldspar (1 mm) with multiple inclusions of biotite (metamict and laths) and plagioclase laths (0.1 mm) indicative of a quenched magma. This suggests that the first phases to crystallize were biotite and plagioclase, the last phases (quenched) were quartz and K-feldspar (Plate 4.3a,b).



Plate 4.2 The groundmass of the mafic xenoliths exhibiting a sieve texture of poikiolitic quartz and K-feldspar with multiple inclusions of biotite and plagioclase laths. (#63112, crossed polars, x32) The subhedral microperthite megacrysts (40 mm) exhibit exsolution textures and are poikiolitically zoned by inclusions of plagioclase (An₈₋₁₃), biotite and quartz. The plagioclase zones are optically continuous suggesting simultaneous crystallization during the growth of the megacryst. The plagioclase zone has myrmekitic intergrowths with quartz and contains biotite laths (2 mm, i.e. larger than the groundmass). The irregular rims of the microperthite commonly have albite overgrowths. Minor muscovite replacement of the microperthite is also observed.

The non-undulose, euhedral, equant quartz megacrysts (8 mm) are rimmed by foliated, undeformed biotite flakes (0.1 mm). Oscillatory zoned, euhedral, columnar plagioclase megacrysts however, lack the biotite rims associated with K-feldspar and quartz megacrysts.

Perhaps the most important textural feature of the mafic xenoliths is the quenching and depletion of the groundmass around megacrysts in the minerals that form the K-feldspar, and quartz megacrysts. This feature, in association with the related biotite foliation of the xenoliths and the plagioclase zoning of the K-feldspar megacrysts, indicates the megacrysts continued to crystallize after emplacement under near-solidus conditions, following the initial quenching of the surrounding groundmass.

Emplacement of the mafic xenoliths within the garnet-biotite granite and the subsequent crystallization of biotite-garnet (cordierite) rims occurred prior to solidification of the host granite. This is supported by biotite schlieren trailing from the xenoliths.

The observation (Section 2.8.2) of sheared porphyritic mafic aplite dykes with boudinaged and biotite-quartz rich layers (schlieren) suggests a possible mechanism of emplacement for the mafic xenoliths within the garnet-biotite granite. The lack of petrographical and geochemical data on such dykes, however, makes interpretation speculative.

4.3.2 Facies Diagram for the Garnet-Biotite Granite Mafic Xenoliths

In the ACF diagram (Figure 4.1) the garnet-biotite granite mafic xenoliths plot just above the plagioclase-biotite tie line which separates I- and S-type granites (White & Chappell, 1977). These S-type granitoid mafic xenoliths, therefore, occur within the subtriangle corresponding to their hosts petrographically observed mineral assemblage, suggesting that they are cognate (i.e. they are genetically related to the garnet-biotite granites which also plot in an identical position (Figures 4.1, 4.2). The ACF diagram (Figure 4.1) also shows that the mafic xenoliths are not related to the country rock xenoliths which plot quite separately, along the muscovite-biotite tie line.

In summary, the ACF diagram suggests the mafic xenoliths of the garnet-biotite granites are cognate, with a hypothetically intrusive emplacement suggested by field and textural evidence. The garnet-biotite (cordierite) rims of the mafic xenoliths will be discussed in Section 4.5.

4.4 APLITIC XENOLITHS FROM THE GARNET-BIOTITE GRANITE

4.4.1 Geology and Petrography of the Aplitic Xenoliths

Two concentrations of large angular aplitic xenoliths occur within the garnet-biotite granite of the Ansons Bay Batholith at Deep Creek, 3 km nortwest of Eddystone Point, and at the southern end of Boulder Point, 6.5 km east-northeast of Mt William. All xenoliths possess a garnetbiotite (cordierite) rim (Plate 2.9a,b), which will be discussed in Section 4.5.

The aplitic xenoliths range in surface exposure from 1 m^2 to >100 m². They are commonly rectangular in outline, with their long axis perpendicular to the mineral foliation of the garnet-biotite granite. Their alignment correlates with the strike direction of dykes within the Ansons Bay Batholith (Figure 2.9) which are also perpendicular to the K-feldspar mineral foliation of the granite. The xenoliths exhibit sharp contacts against the granite and are outlined by a garnet-biotite (cordierite) rim up to 40 cm wide (Plate 2.9a). The Deep Creek xenoliths are sparsely phyric (K-feldspar) compared to the equigranular xenoliths of Boulder Point.

Stained hand specimens (63090, 63091, 63093) illustrate the dominance of K-feldspar (41-58%) over quartz (33-42%) and plagioclase (10-22%). (Complete modal analyses are presented in Appendix 1.) Biotite occurs as the major mafic phase (4.4-1.4%) together with muscovite (0-2.0%).

Petrographically the xenoliths resemble the alkali feldspar granites of the Ansons Bay Batholith (Section 2.7). Their dominant mineralogy consists of granophyric intergrowths of quartz plus subhedral-anhedral micro-mesoperthitic K-feldspar and microcline (<5 mm, up to 30 mm in the phyric varieties). Subhedral, equant albite-oligoclase (An_0-An_{30}) crystals less than 5 mm in diameter occur sparsely throughout the phyric xenoliths, becoming more abundant in the equigranular varieties (see modal analyses, Appendix 1). The micas are equally divided between biotite laths (<2 mm) and muscovite. The medium grained muscovites have a secondary appearance, replacing the feldspars. Other minor, but very important mineralogical phases consist of subhedral-anhedral sericitized Fe-rich cordierite (<1.5 mm), and subhedral almandine-rich garnets (<2 mm).

4.4.2 Facies Diagrams for the Aplitic Xenoliths

The ACF diagram (Figure 4.1) illustrates the aplitic xenoliths plotting within the three-phase plagioclase-muscovite-biotite triangle, close to the biotite-muscovite tie line. Their relative position within this subtriangle is identical to that of the alkali feldspar granites (Figure 4.2).

The similarity in hand specimen, petrography and geochemistry of the xenoliths with the alkali feldspar granites of Mt William and Boulder Point, together with their rectangular outlines, their restricted occurrence, and

parallel orientation to leucocratic dykes throughout the area is interpreted to indicate that the xenoliths are dismembered alkali feldspar dykes. Less disrupted dykes of similar composition have been observed in the Furneaux Group (E. Reid, pers. comm., 1982).

These early intrusive alkali feldspar dykes would have intruded the partially crystalline garnet-biotite granite in a molten state (as suggested by the granophyric intergrowths). Their different viscosity and intrusive temperature would have caused solidification and prevented assimilation of the dykes with the host garnet-biotite granite. The enrichment of the alkali feldspar dykes in volatiles from the melt, and the changing intrusive conditions may have provided the necessary prerequisites for the formation of the garnet-biotite (cordierite) rims to the dismembered dykes.

4.5 GARNET-BIOTITE (CORDIERITE) RIMS TO XENOLITHS

4.5.1 Geology and Petrography

Mafic garnet-biotite (cordierite) concentrations have been mentioned in Sections 2.6, 4.3 and 4.4 as outlining the margins of igneous xenoliths or occurring as layers and isolated accumulates within/the garnet-biotite granite (Plates 2.12a,b; 2.13a,b).

Petrographically the composition of the mafic concentrations contain 25% biotite, 20% garnet, 15% cordierite, 15% plagioclase, 15% quartz and 10% K-feldspar. The dark brown, medium grained biotite occurs as both subhedral columnar and anhedral metamict flakes. Inclusions of apatite, monazite, ilmenite, zircon and rutile are characteristic. Biotite commonly occurs as aggregates up to 6 mm or as mantles around the garnets (Plate 4.3a,b).

Euhedral-subhedral almandine-rich garnets up to 8 mm in diameter and containing multiple fractures filled with brown biotite are the second most abundant mineral forming the rims to the igneous xenoliths.



Plate 4.3(a) Garnet-biotite-cordierite mineral assemblage of #63055, plane polarized light (x 15).



Plate 4.3(b) Garnet-biotite-cordierte mineral assemblage of #63055, cross polarized light (x 15).

Garnet inclusions consist of brown biotite, quartz, opaques and minor secondary green biotite.

Extremely fresh subhedral cordierite crystals up to 6 mm in length with minor sericitic alteration and simple twinning are common to most mafic rims (63055). Cordierite is characteristically free of inclusions.

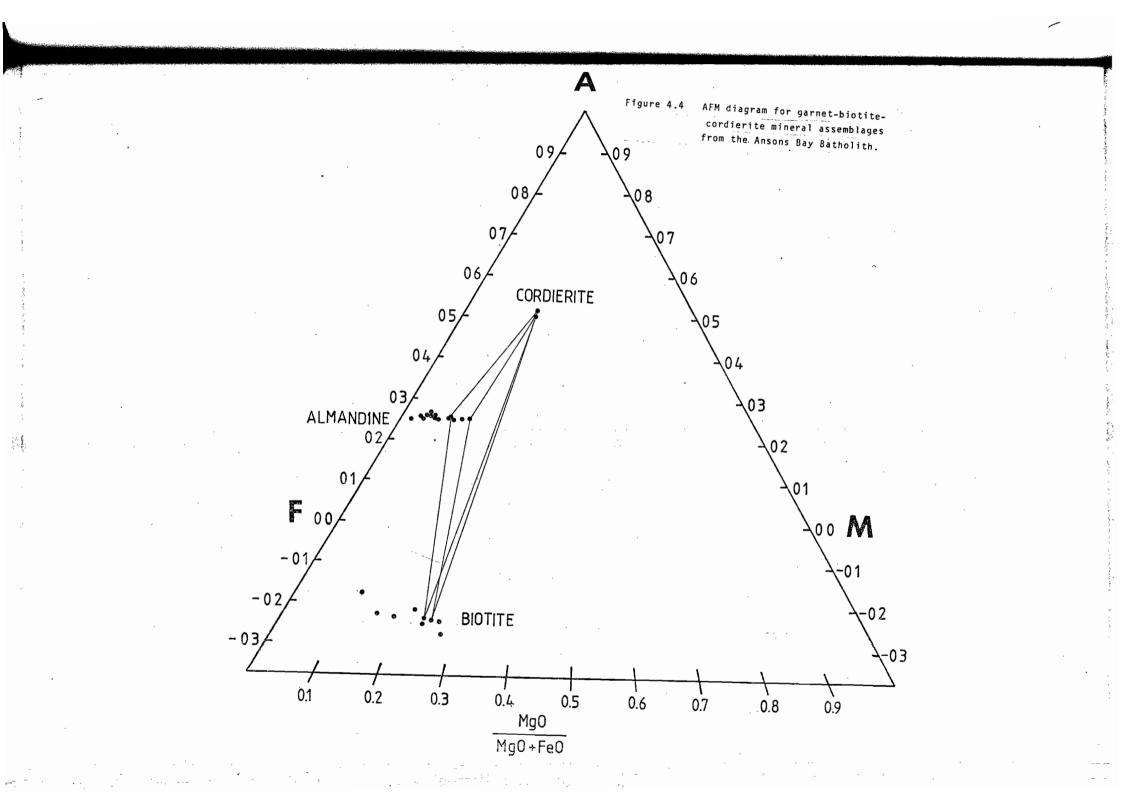
The equant, medium grained (up to 5 mm), subhedral, oscillatory zoned (rim An₂₁, core An₃₇) plagioclase crystals with albite and Carlsbad albite twinning commonly have altered sericitized cores and rims with reversed twinning. The interstitial quartz and K-feldspar are anhedral, up to 3 mm long, with inclusions of garnet, biotite and plagioclase. The quartz grains show minor undulose extinction.

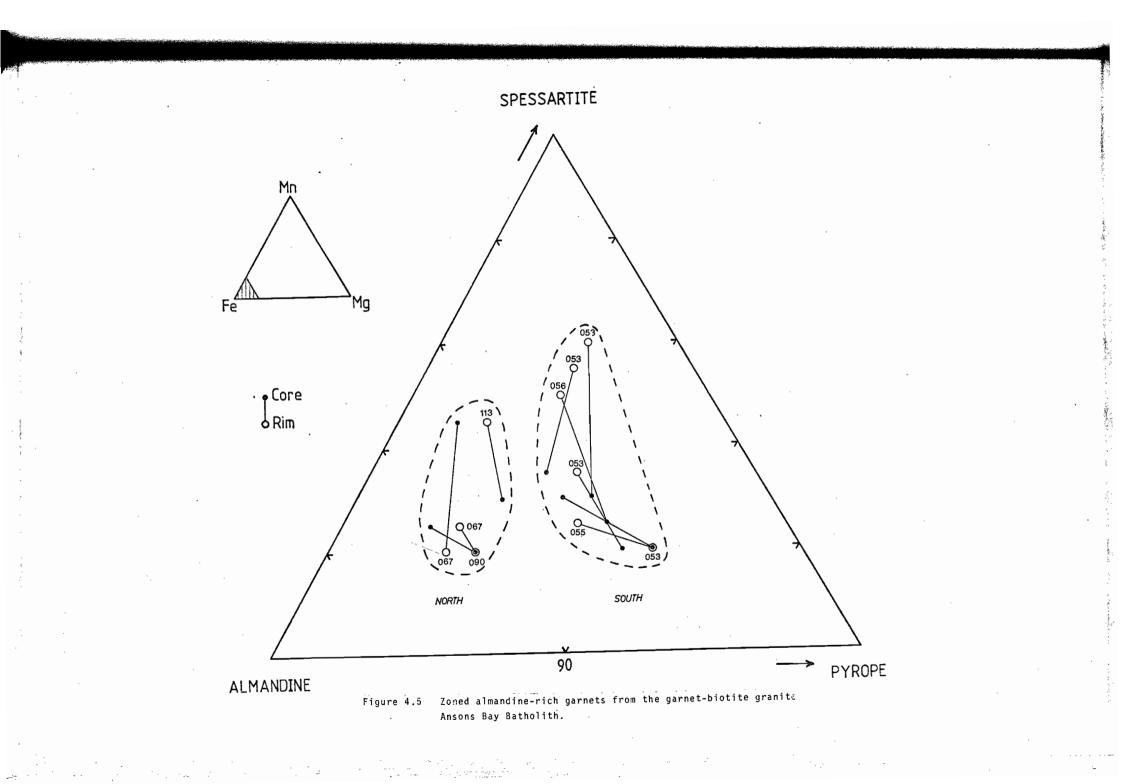
4.5.2 Garnet Geochemistry

Garnet-biotite (cordierite) microprobe analyses have been used in geothermometry (Section 5.1) and are tabulated in Appendix 3. Their compositions have been plotted on an AFM diagram (Figure 4.4) and co-existing three-phase tie lines between minerals in equilibrium have been drawn.

Figure 4.4 illustrates the iron-rich nature of the garnet, biotite and cordierite. The iron-rich garnets plot as two separate fields in the almandine garnet region (Figure 4.5). Of the garnets analysed, those from north of Eddystone Point are more Fe-rich than those from south of Eddystone Point. This corresponds with the biotite geochemistry which exhibits a similar trend (Figure 6.4). The analysis of garnets from xenoliths are identical to the host rock, further confirming the cognate nature of the xenoliths.

The garnets, apart from plotting into two separate fields, also exhibit either normal or inverse zoning (Figure 4.5). Inversely zoned garnets are the most common variety and are characterized by decreasing Mg/(Mg+Fe) ratios and increasing manganese contents from core to rim. Normally zoned garnets possess the reverse relationship, i.e. increasing





Mg/(Mg+Fe) ratios and decreasing manganese contents from core to rim (Figure 4.5).

Dietvorst (1982), Tracy *et al.* (1976), and Thompson (1976) believe that the growth of inversely zoned garnets is due to a continuous Fe-Mg-Mn exchange reaction between garnet and biotite. Such reactions are inferred by Froese (1973) and Dietvorst (1982) to occur at low water pressures $-P_{\rm H_2O} \simeq 0.5 P_{\rm total} -$ under retrograde conditions.

The majority of the garnets associated with the garnet-biotite granite are inversely zoned, almandine-rich garnets that formed under retrograde conditions at low water pressures.

The P-T conditions of formation for the igneous xenoliths and their garnet-biotite (cordierite) rims may be inferred from divariant mineral reactions in the system SiO_2 -KAlSi $_3O_8$ -NaAlSi $_3O_8$ -CaAl $_sSi_2O_8$ -H $_2O$. Their stability field is assumed to be outside that of muscovite and therefore muscovite-bearing assemblages have been omitted from the following discussion.

Where a silicate liquid is involved, quartz, alkali feldspar, oligoclase-andesine, and H_2O may be thought of as participating according to the following generalized reaction (Abbott, 1978):

quartz + alkali feldspar + plagioclase 🟅 liquid

with $a_{H_2O} < 1$.

This reaction represents an oversimplification of the possible liquidus reactions that may occur in the system SiO_2 -KAlSi $_3O_8$ -NaAlSi $_3O_8$ -CaAl $_2Si_2O_8$ -H $_2O_8$ depending on P_{H2O} and a_{H2O} (Abbott & Clarke, 1979).

In terms of the P-T diagram (Figure 4.6) for an $a_{H_2O} \sim P_{H_2O}/P_{total} =$ 1.0 and 0.6 the limiting divariant P-T field for the igneous xenoliths and their garnet-biotite (cordierite) rims is approximately 700°C and <3 kb pressure. This temperature agrees with that obtained by garnet-biotite geothermometry (Section 5.1) and the accompanying pressure of <3 kb correlates well with the low pressure envisaged for the formation of the

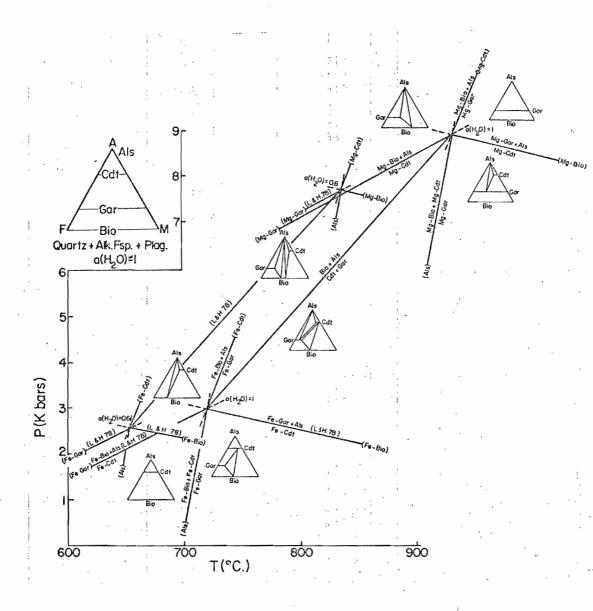


Figure 4.6

P-T diagram for the system $A(A1_2O_3-K_2O-Na_2O-CaO)$ -F(FeO)-M(MgO) projected through H₂O, quartz, alkali feldspar and plagioclase for two activities of H₂O, $a(H_2O) = 1.0$ and 0.6 (from Abbott & Clarke, 1979).

agmatic migmatite contact and the garnet-biotite (cordierite) rims.

In summary, the P-T conditions of emplacement of the plutons of the Ansons Bay Batholith from geological considerations such as the rims to xenoliths, and dykes suggest a high level of emplacement of the granites at approximately 700° C and 1 kb.

.:. -

Έ.

Chapter 5

GEOTHERMOMETRY

5.1 INTRODUCTION

Temperature calculations were attempted using both garnet-biotite (cordierite) and feldspar geothermometry. Analyses were performed using the electron microprobe at the University of Tasmania, and analyses have been tabulated in Appendix IV.

5.2 GARNET-BIOTITE (CORDIERITE) THERMOMETRY

The results of garnet-biotite geothermometry, calculated according to Ferry & Spear (1978), and Thompson (1976) have been tabulated in Table 5.1. They show that temperature determinations according to Ferry & Spear (1978) are consistently lower than those of Thompson (1976). Table 5.1 also illustrates the necessity of having mineral pairs that are in equilibrium, for geothermometry. For example, the rims of the zoned garnets, rather than the cores, are more likely to be in equilibrium with neighbouring biotites. For similar reasons only geothermometry on inversely zoned garnets have been tabulated. Therefore geothermometry using inversely zoned garnet rims and neighbouring biotites should provide the correct temperatures of formation (Dietvorst, 1982).

Average temperatures of $700^{\circ} \pm 15^{\circ}$ C were determined for inversely zoned garnet rims and neighbouring biotites compared to $875^{\circ} \pm 50^{\circ}$ C for inversely zoned garnet cores and the same neighbouring biotites. The lower temperature of $700^{\circ} \pm 15^{\circ}$ C is presumed to represent the emplacement temperature of the garnet biotite granites.

Geothermometry using coexisting garnet-cordierite-biotite mineral assemblages (63055) were not consistent with garnet-biotite geothermometry. Possible reasons for this disparity are:

Specimen	Garnet (rim)		Garnet (core)	
	Ferry & Spear, 1978	Thompson 1976	Ferry & Spear, 1978	Thompson, 1976
63053	756 714	715 685	886 1029	801 891
63056	775	728	1062	911
63113	619 661 633	616 647 626	788 847 808	736 776 750
63067	834	767	1036	895
Average	713	683	922	824

Table 5.1

Table 5.2

X _{P1}	X _{AF}	Temperature ^O C
0.33	0.13	,650
0.56	0.20	675
0.51	0.23	750
	0.33	0.33 0.13 0.56 0.20

 X_{P1} = mole fraction albite in plagioclase X_{AF} = mole fraction albite in K-feldspar and such a first the first second secon

- 4

- The minerals are not in equilibrium (i.e. cordierite out of equilibrium).
- 2. More probe data on coexisting rims are necessary.

3. Fe³⁺ is present in the biotites.

The importance of Fe^{3+} in biotites is important since in the equation

$$\zeta_{\rm D}^{\rm Bi} = \left(\frac{{\rm Fe}^{2+}}{{\rm Mg}}\right)^{\rm Gt} \times \left(\frac{{\rm Mg}}{{\rm Fe}^{2+}}\right)^{\rm Bi}$$

we assume that the $\Sigma Fe = Fe^{2+}$. If, however, there is a lot of Fe^{3+} in the biotite then the ΣFe as Fe^{2+} gives a much lower K_D than the real one (i.e. a much higher temperature than the real temperature).

5.3 FELDSPAR GEOTHERMOMETRY

Feldspar geothermometry using the graphical technique of Brown & Parsons (1981), for P = 1 kb, was attempted on the electron microprobe analyses of feldspars (Appendix IV) from the granitoids of the Ansons Bay Batholith.

The technique is based on the distribution of sodium between coexisting plagioclase and K-feldspar crystals. Temperatures were calculated from Figure 2 of Brown & Parsons (1981). The temperature range obtained using the hundreds of probe analyses was consistently lower than the magmatic temperatures expected for the crystallization of plagioclase and K-feldspar from a magma (Carmichael *et al.*, 1974). Probe analyses from slides 63064, 63066, 63086 were the only exceptions to these low temperatures (see Table 5.2). Their temperatures are consistent with those obtained by garnet-biotite geothermometry for the Ansons Bay Batholith.

93

. .

For accurate feldspar geothermometry it is imperative that the feldspar pairs be in equilibrium. Petrographic descriptions have already suggested that equilibrium between the feldspars is not always evident. Plagioclase, for example, exhibits oscillatory zoning and hence has a variable composition. K-feldspar on the other hand exhibits perthitic exsolution which reduces the Na component of the K-feldspar and therefore lowers the calculated temperature. Secondary sericitic and muscovite replacement of feldspars also suggests some later subsolidus re-equilibration resulting in compositional readjustment.

In summary, the anomalously low temperatures obtained from the graphical technique of feldspar geothermometry proposed by Brown & Parsons (1981) may have resulted from the variable plagioclase composition within individual crystals, perthitic exsolution or subsolidus reequilibration or any combination of these factors. The temperatures obtained, with the exceptions of 63064, 63066, and 63086, therefore do not represent true magmatic temperatures.

94

....

Chapter 6

GEOCHEMISTRY OF THE ANSONS BAY BATHOLITH

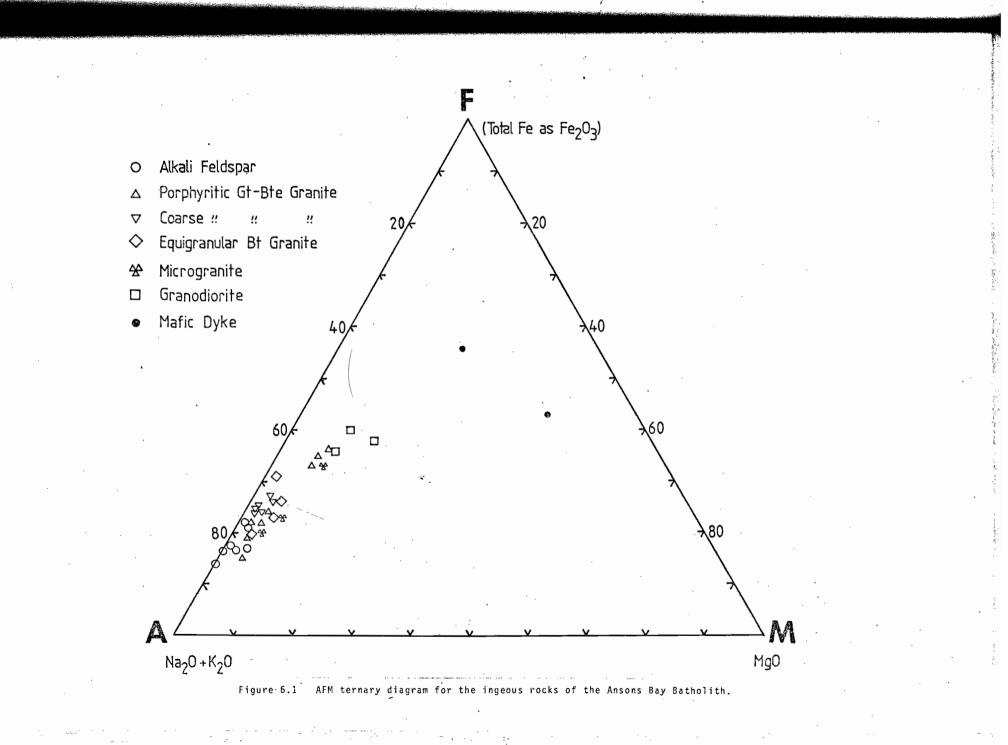
6.1 INTRODUCTION

A total of 63 geochemical analyses of Mathinna Beds, granodiorites, microgranites, granites, aplites, dolerites, lamprophyres, and various xenoliths were performed in order to evaluate, through major and trace element modelling, the processes involved in the petrogenesis of the Ansons Bay Batholith.

Analyses of major, trace and rare earth elements were determined at the University of Tasmania (Appendix 2). Major and trace elements were obtained by XRF analysis using both glass discs and pressed pills respectively, after Norrish & Hutton (1969), on a Philipps PW1410 manual X-ray spectrometer, automated by a TRS-80 microcomputer. REE analyses were performed by Dr N.C. Higgins using an ion-exchange XRF technique introduced by Eby (1972) and modified by Fryer (1977). REE precision is better than 10%, and commonly less than 5% for all elements, with a detection limit of approximately 0.3 ppm for all the REE. CIPW normative calculations are tabulated and presented in Appendix 4.

6.2 MAJOR ELEMENT VARIATION

The granitoids, dolerites and lamprophyres of the Ansons Bay Batholith (ABB) lie on the calcalkaline trend of Tilley (1950) (Figure 6.1). The granitoids, however, are more typically confined to the compositionally restricted calcalkaline types of Pitcher (1979). In the AFM plot (Figure 6.1) the bulk of the granitoid analyses plot into two separate fields. The two fields isolate the granodiorites from the other granitoids. The AFM diagram also provides some evidence for the granitoids having undergone differentiation or similar fractionating processes during their genesis.



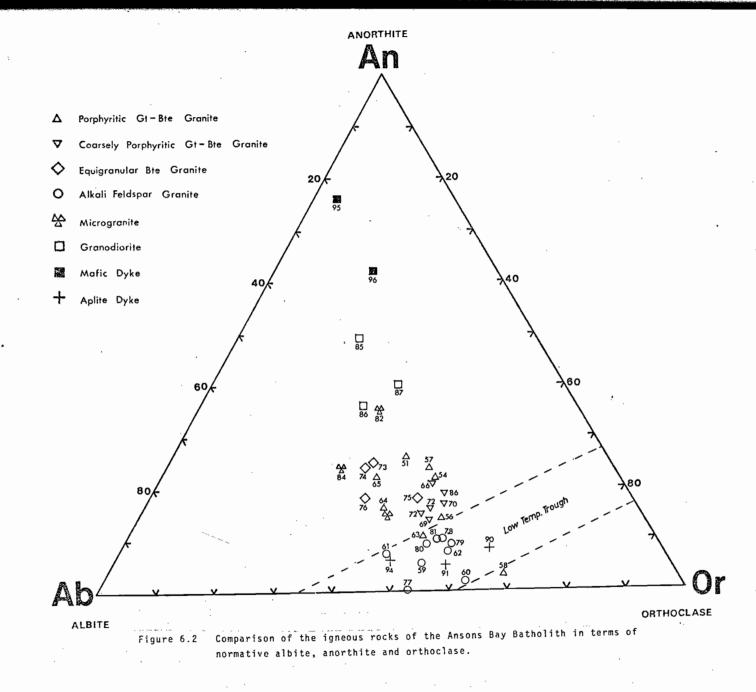
The An-Ab-Or ternary diagram (Figure 6.2) illustrates the individuality of the granodiorite relative to the other granitoids of the ABB, and confirms the trend in Figure 6.1, consistent with the Blue Tier Batholith (Cocker, 1977; Higgins *et al.*, 1982). Figure 6.2 also indicates that the alkali feldspar granite plus the aplitic dykes and related xenoliths lay in a low temperature trough relative to the other granitoids.

Although the granitoids appear to plot close to the minimum point for 1 kb P_{H_2O} in the Qtz-Ab-Or ternary diagram (Figure 6.3), the An-Ab-Or diagram suggests they lie above the cotectic surface and are non-minimum melts (except the alkali feldspar granites which plot in the low temperature trough). A similar trend is observed for the granite plutons of the Blue Tier Batholith (Higgins *et al.*, 1982).

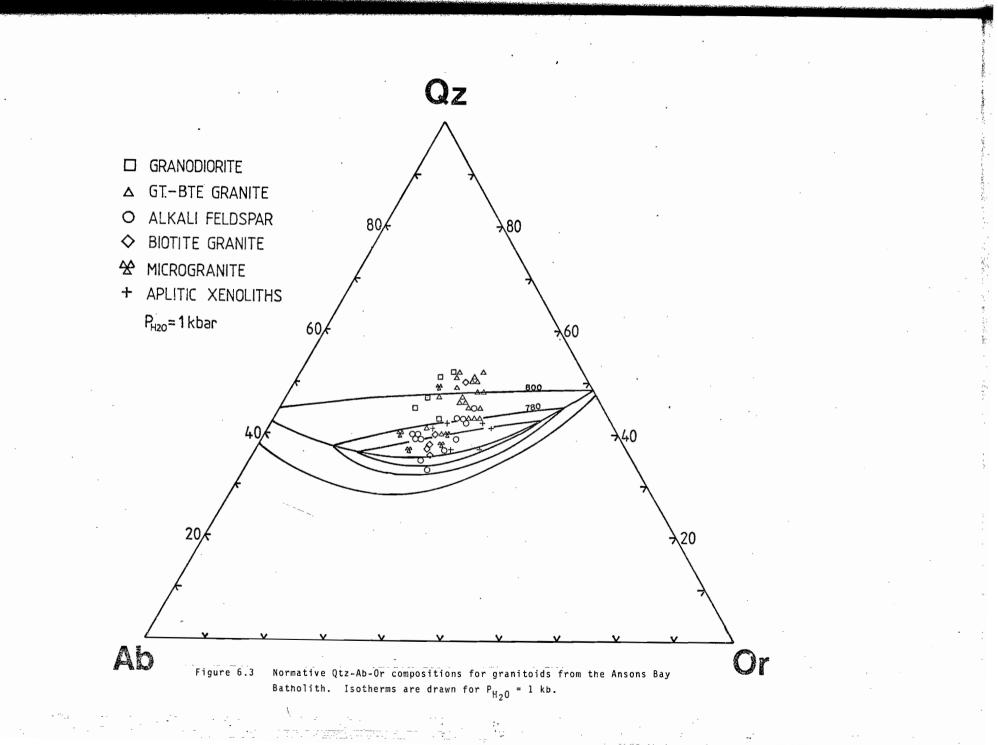
A plot of Mg/(Mg+Fe) ratios of biotite against whole rock SiO_2 (Figure 6.4) once again illustrates the difference between the granodiorites and granitoids, as well as dividing the ABB into north and south granitic regions. The southern region, south of Eddystone Point, has the lower SiO_2 and higher Mg[#] values and includes the less porphyritic garnetbiotite and biotite granites. The Musselroe Point microgranites are also included within this field. The northern region, which includes Eddystone Point, has higher SiO_2 and lower Mg[#] values, and encompasses the more coarsely grained and porphyritic biotite-, garnet-biotite, and alkali feldspar granites plus their related xenoliths.

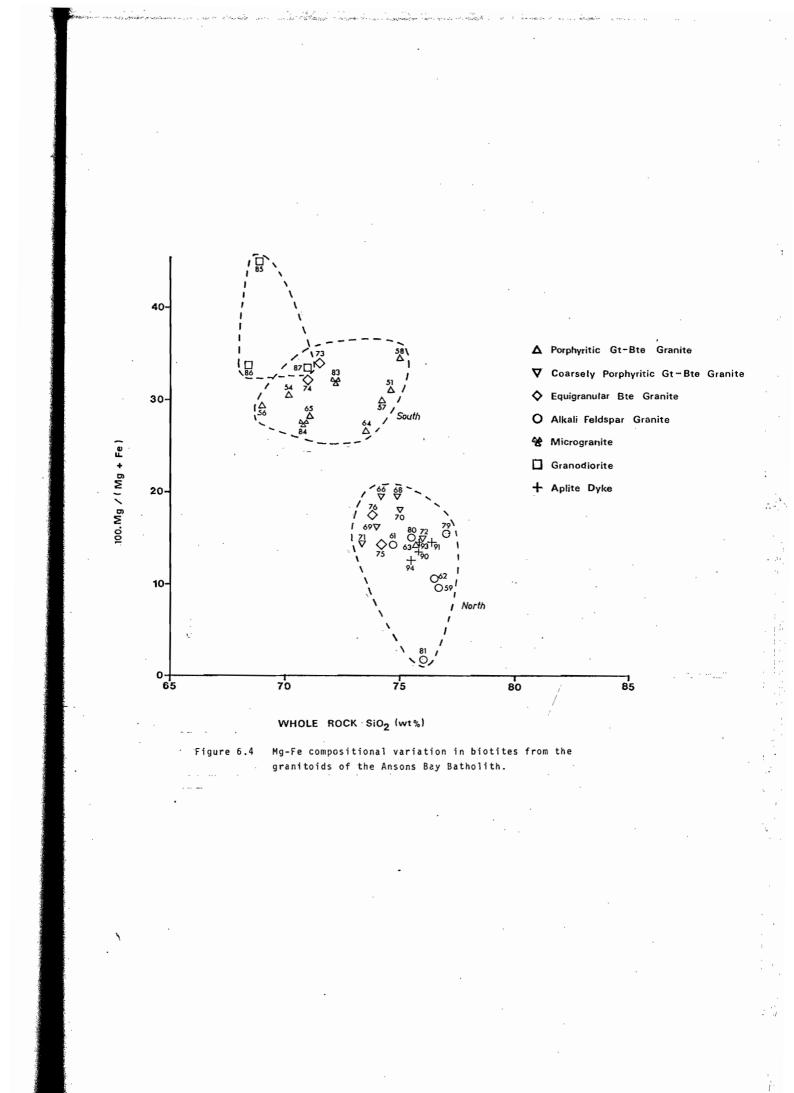
In Chapter 2, Table 2.1, an attempt was made to characterize the ABB granitoids according to the I- and S-type criteria, using field relationships, petrographic features, and geochemical parameters (Chappell & White, 1974; Hine *et al.*, 1978).

Based on the 20 or so criteria listed in Table 2.1 it was concluded that the granodiorites are I-type, the biotite, alkali feldspar and microgranites are predominantly S-type and the garnet-biotite granites are unquestionably S-type.



and a second second





(1) A set of the se

.

The computer printouts of Figure 6.5a-f depict the variation of major elements with increasing SiO2 content. The various granitoid fields have also been outlined to emphasize the chemical variation between plutons. To avoid any unnecessary confusion of lines the overlapping biotite- and garnet-biotite granite fields have been combined as have the alkali feldspar granites and their related xenoliths. The first and most obvious trend is the increase in silica from granodiorite to microgranite to garnetbiotite granite to alkali feldspar granite. Within this trend iron, aluminium, titanium, and calcium decrease regularly with increasing silica as does magnesium to a lesser degree. Potassium, however, increases with silica as does sodium. The major element geochemistry also divides the biotite- and garnet-biotite granites into northern and southern regions, but to save ambiguity of symbols this has not been shown in Figure 6.5. The higher silica content of the northern region has lower iron, aluminium, titanium, calcium and magnesium and higher potassium relative to the southern region.

In summary, the major element geochemistry separates the granodiorite from the other granitoids, the latter however appear to be related in the order microgranite, garnet-biotite granite, and alkali feldspar granite. The biotite- and garnet-biotite granites can also be further subdivided into northern and southern regions on major element geochemistry.

These major element variations are similar to those reported from many granitic provinces (e.g. Sierra Nevada - Bateman & Dodge, 1970; West Germany - Emmermann *et al.*, 1975; France - Fourcade & Allegre, 1981).

101

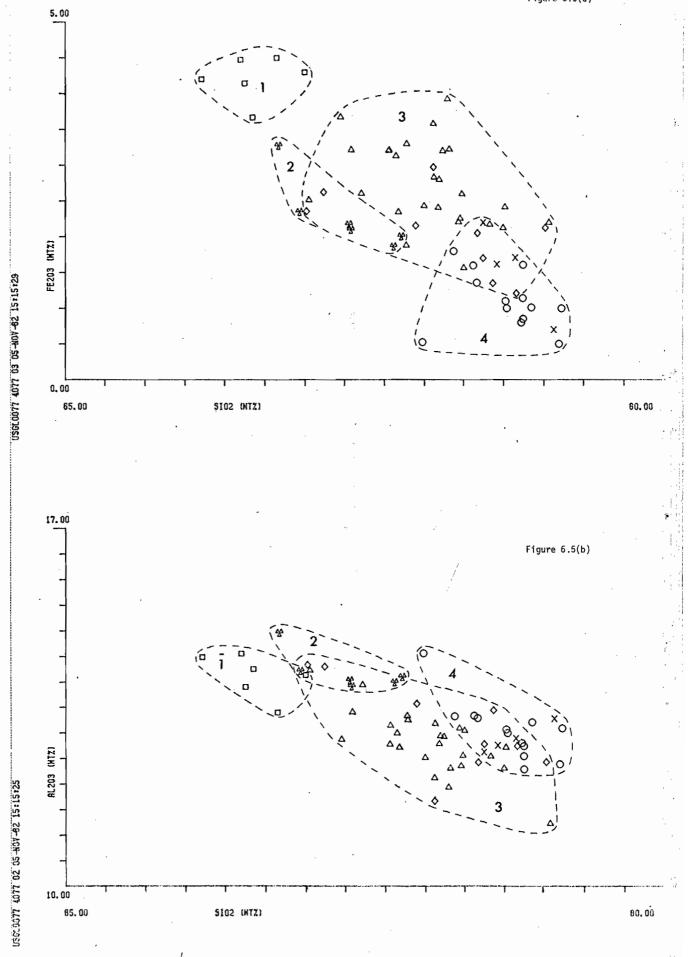
----;*

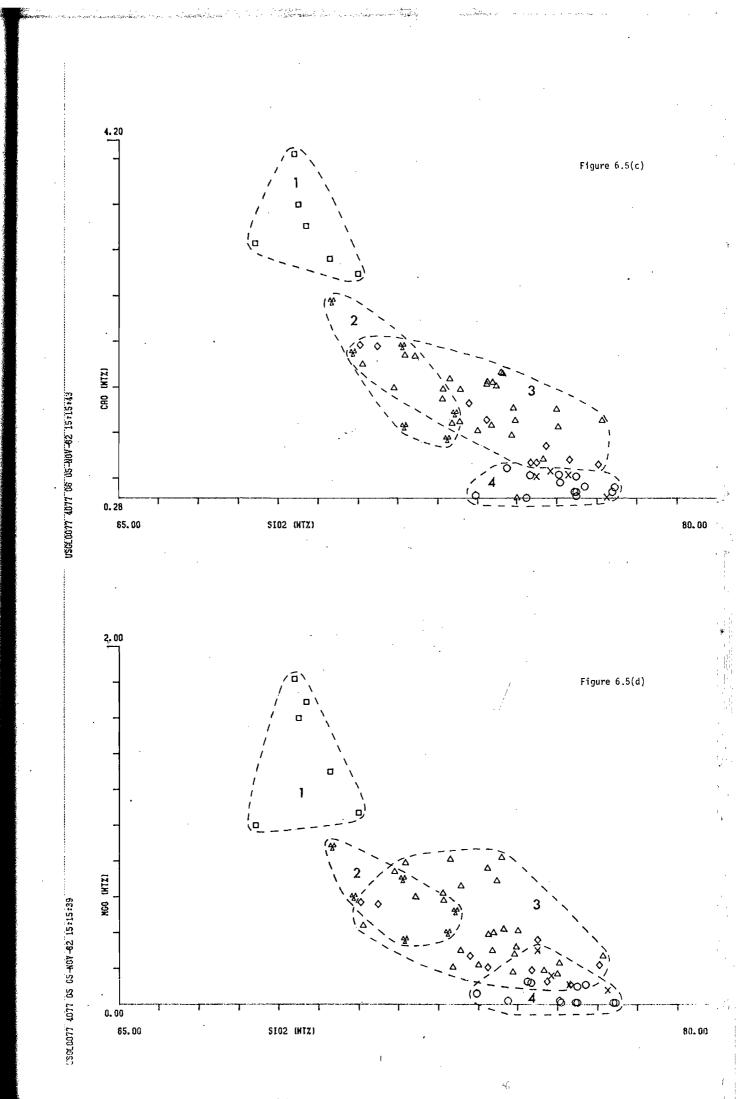
-- Śģ

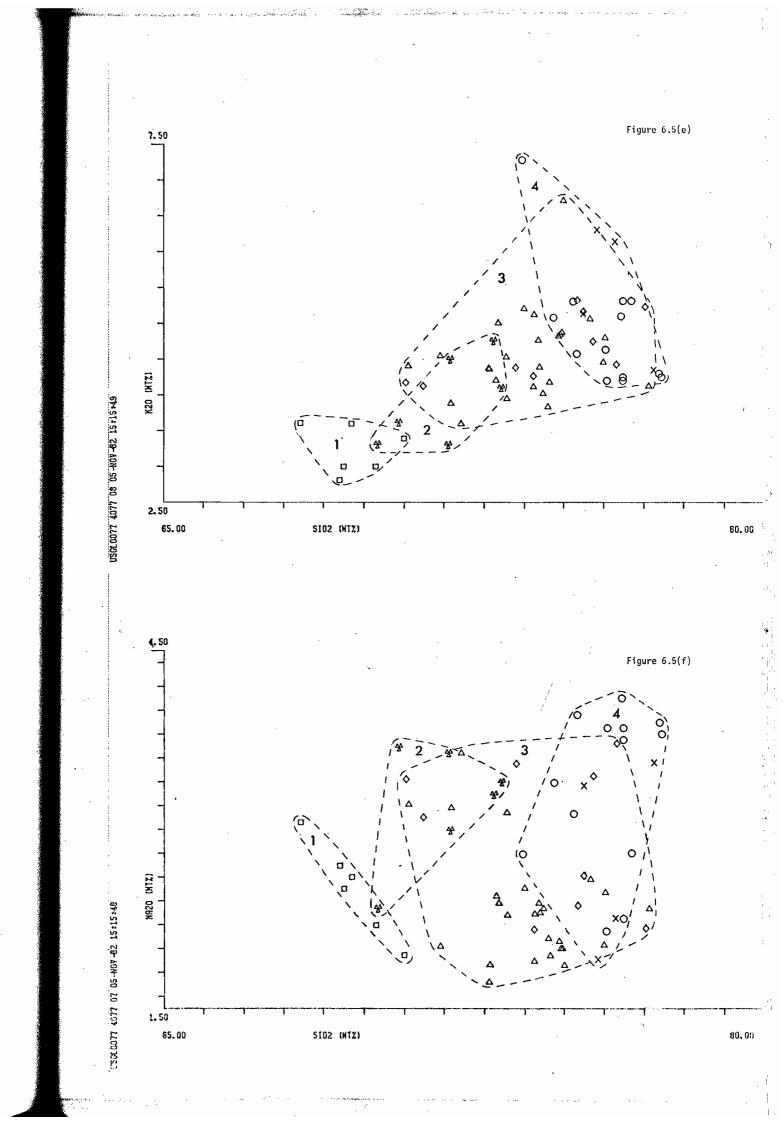
Figure 6.5(a-g)

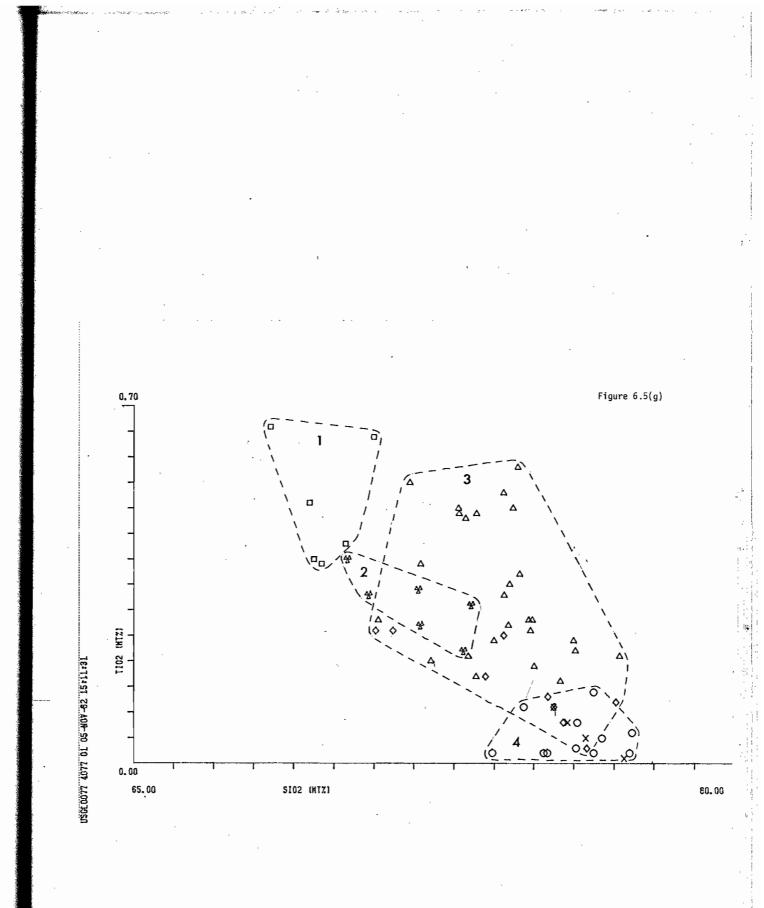
Variation diagrams for the major elements vs SiO₂. Field 1 • granodioriles, Field 2 • microgramite, Field 3 • biotite, garnet-biotite granites, Field 4 • alkali feldspar granites and related xenoliths.

Figure 6.5(a)









L

ġ,

6.3 TRACE ELEMENT VARIATION

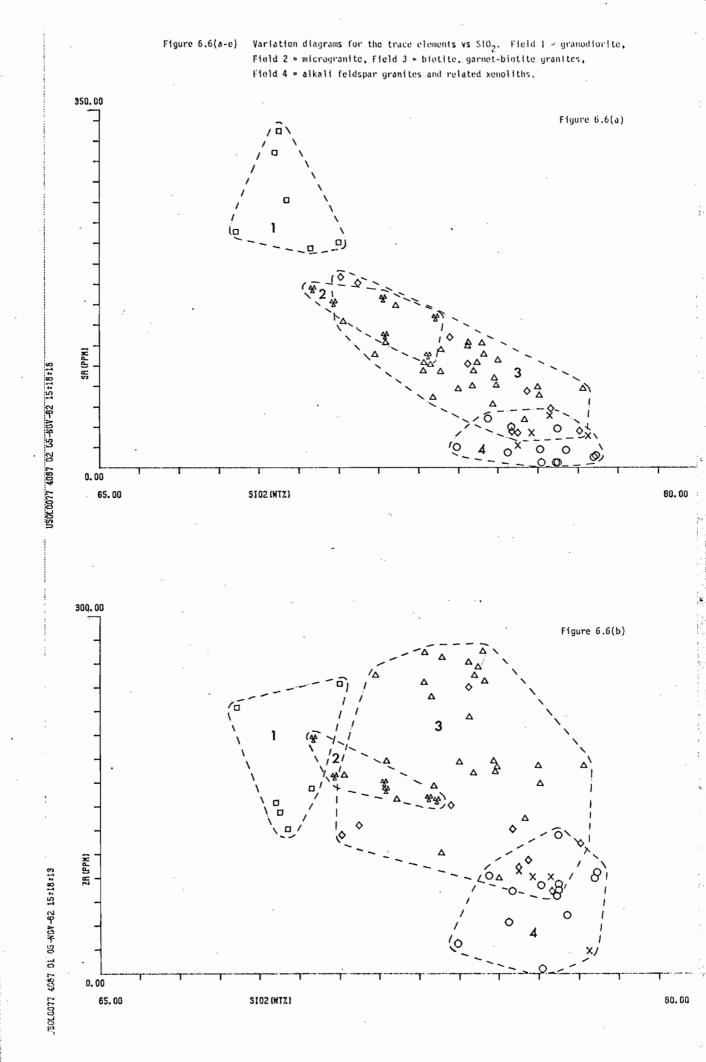
Trace element trends appear consistent with major element variations. Figure 6.6a-e depict the variation in trace elements with increasing silica from granodiorite to alkali feldspar granite. Within this trend strontium and barium decrease regularly with increasing silica as does zirconium but to a lesser degree. Rubidium on the other hand, increases with increasing silica.

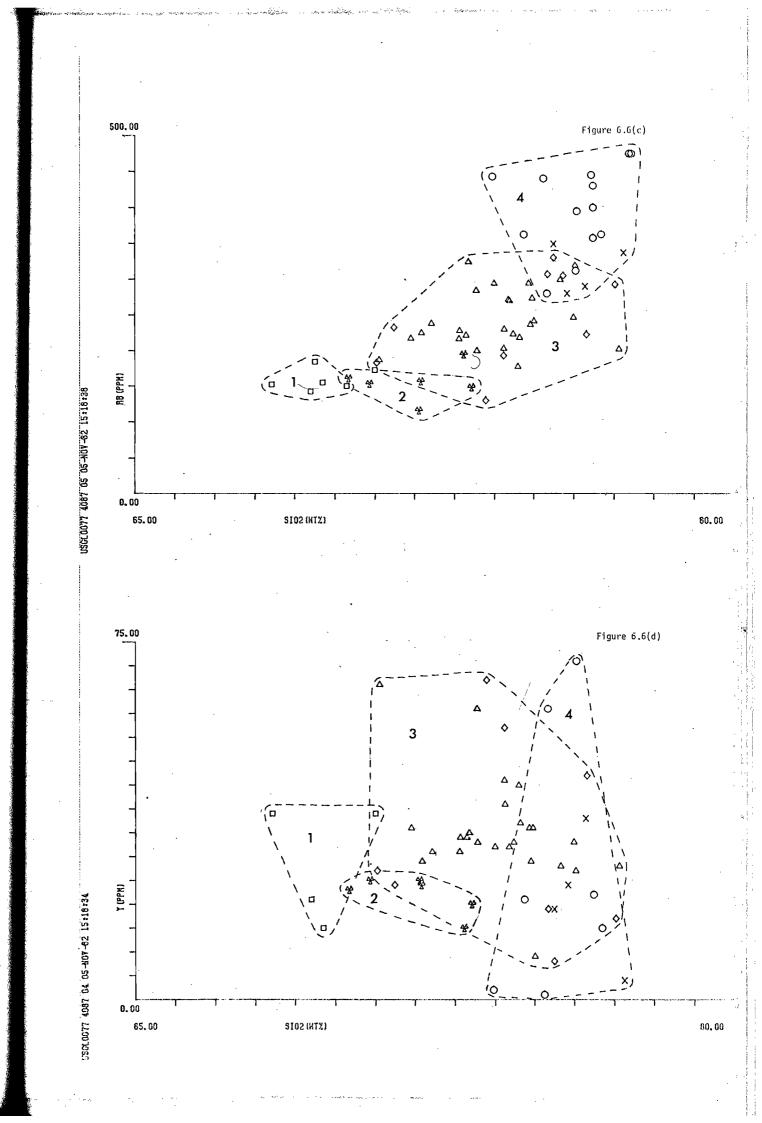
The trace elements like the major elements separate the granodiorites from the other granitoids which once again define a common trend and appear related. The linear variation of these granitoids relative to silica suggests the possibility that fractional crystallization may link the microgranite, biotite-, garnet-biotite, and alkali feldspar granites.

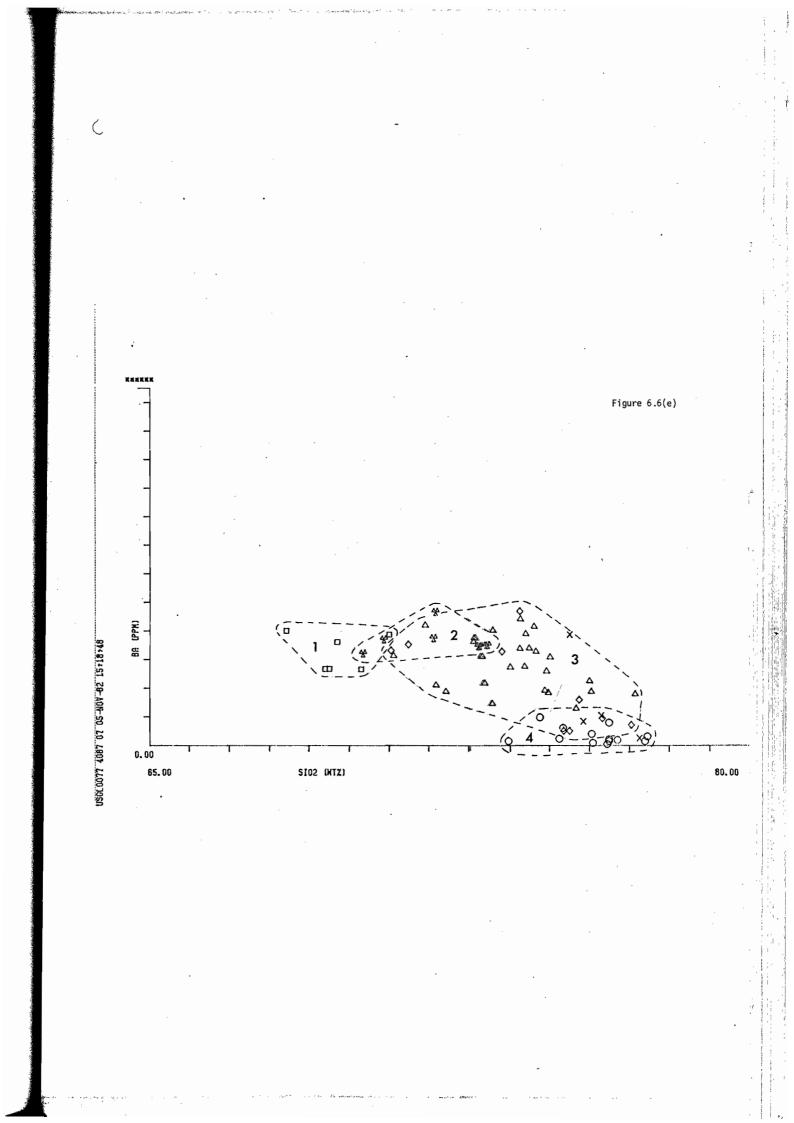
The variation diagrams of Figures 6.7a-d have been prepared to provide some insight into the crystallization processes operative within each of the granitoids of the ABB. Fractionation vectors (after Higgins *et al.*, 1982) on each diagram have been calculated assuming the fractionation of one crystal phase at a time, so that the coincidence of sample trends and fractionation vectors will indicate possible fractionating phases.

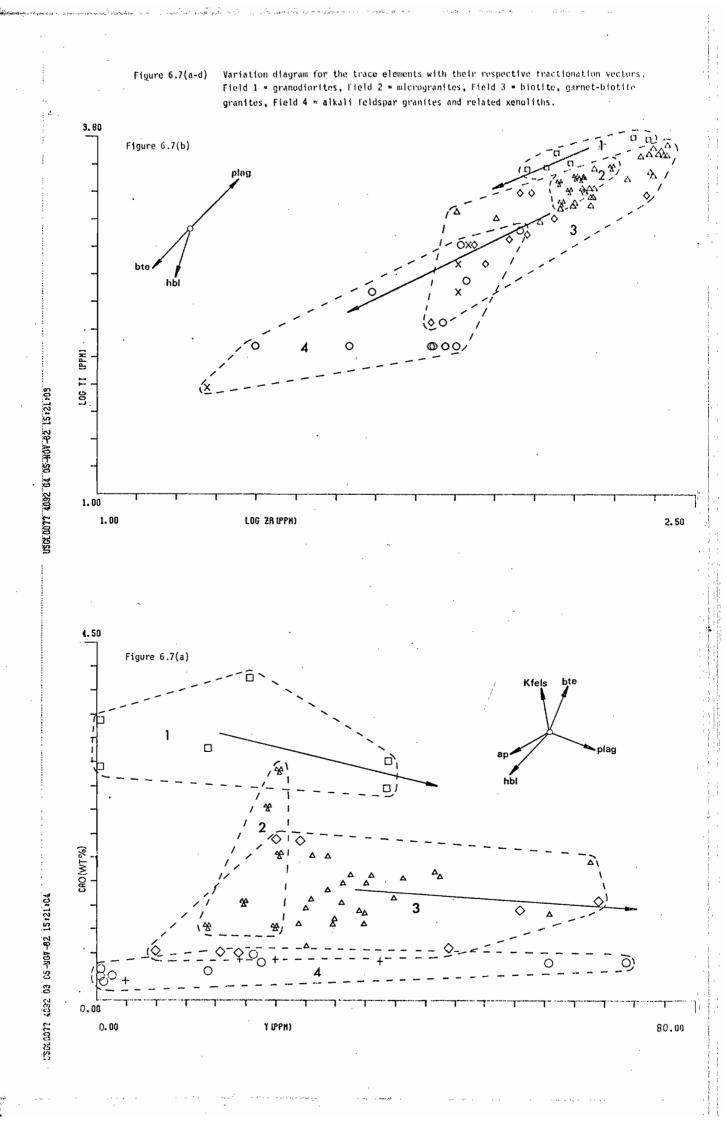
The CaO/Y plot (Figure 6.7a) illustrates the similarity in granitoid trends. The likely fractionating phase for decreasing CaO and increasing Y and SiO₂ (see arrow, Figure 6.7a) in both the granodiorite and the granites is plagioclase. This is in contrast with granodioritic trends for the Blue Tier Batholith (Higgins *et al.*, 1982) where hornblende and apatite have been suggested as the fractionating phases within the granodiorite using a CaO/Y plot, although the number of samples used in this study were fewer. The granitoids possess similar fractionation trends on a $TiO_2/2r$ plot (Figure 6.7b) for biotite fractionation, and further suggest possible biotite and hornblende fractionation in the granodiorites. Trends in Ba/Sr and Ba/Rb plots (Figure 6.7c,d) reflect K-feldspar fractionation

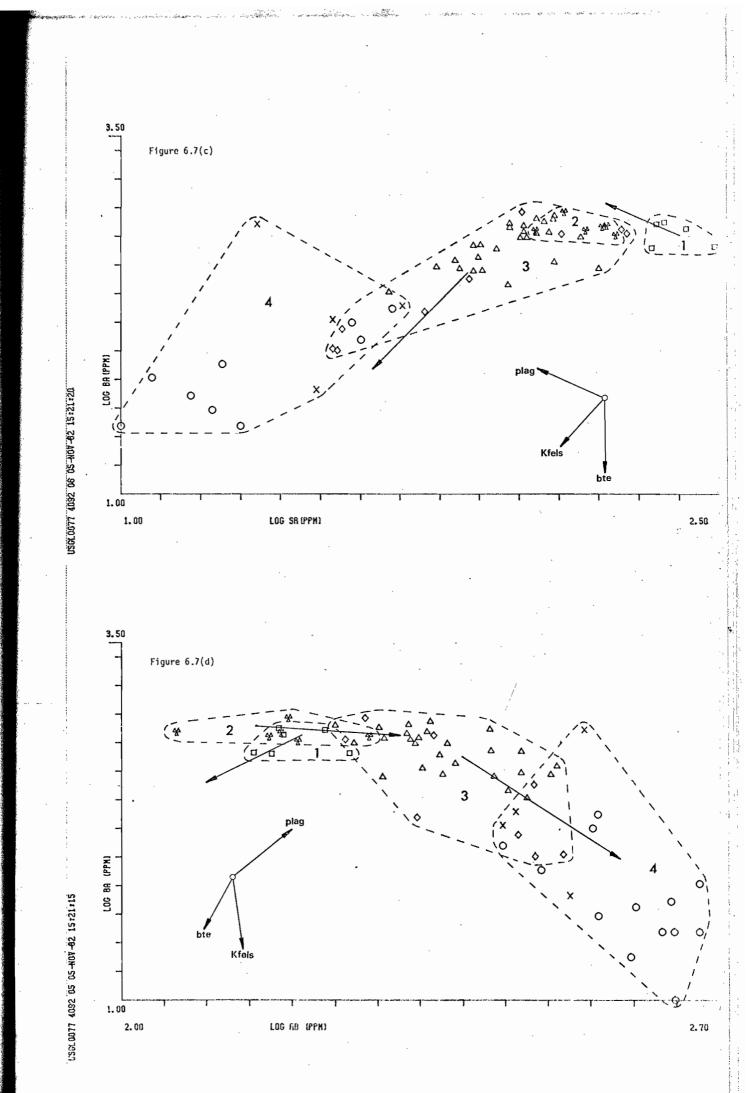
Зį,











and the set of the set

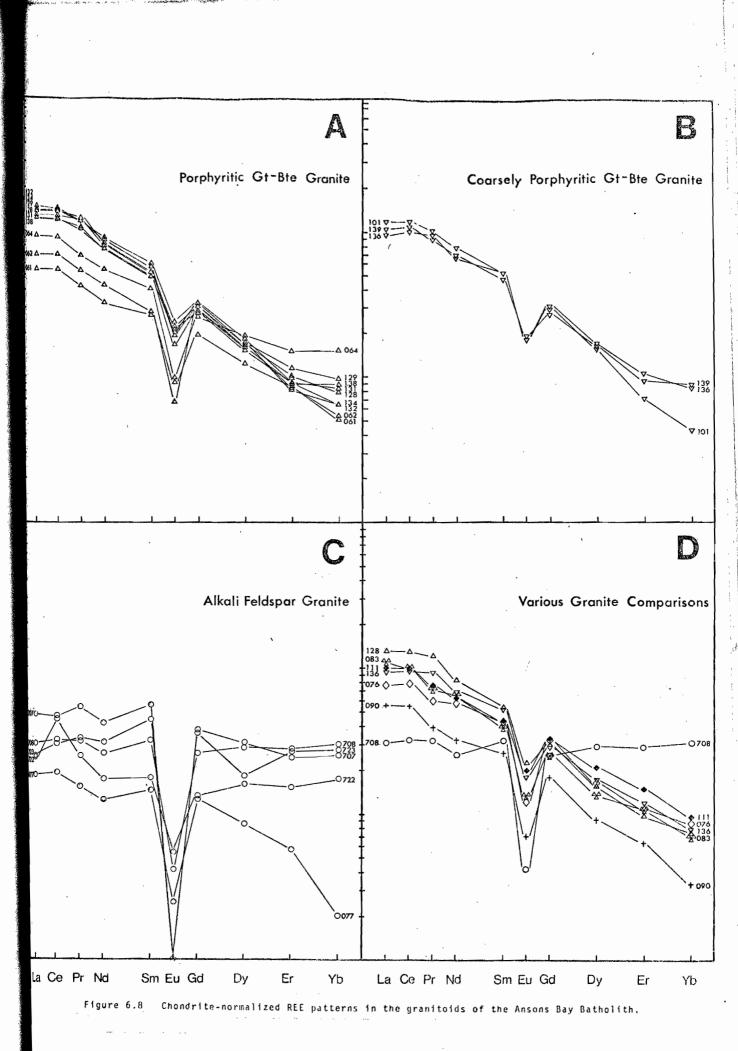
within the biotite-, garnet-biotite and alkali feldspar granites. The alkali feldspar granites may however have been Rb enriched and Sr depleted during hydrothermal alteration (Higgins *et al.*, 1982). The Ba/Sr plot (Figure 6.7c) also illustrates that plagioclase fractionation is important in both the granodiorite and the microgranite. The Ba/Rb plot (Figure 6.7d) however, illustrates the importance of biotite fractionation over plagioclase fractionation in the granodiorites.

In summary, the geochemical trends observed in the granodiorite may be explained by the fractionation of plagioclase, biotite and possibly hornblende, whilst K-feldspar, plagioclase and biotite fractionation explain the chemical trends in the biotite-, garnet-biotite and alkali feldspar granites. Petrographic evidence for the cessation of hornblende fractionation was mentioned in Section 2.3.1.

Major and trace element geochemistry emphasizes the individuality of the granodiorites relative to the other granitoids in the ABB. It also suggests that the microgranites may have undergone different fractionating processes relative to the biotite-, garnet-biotite and alkali feldspar granites. This latter group of granitoids define a common trend suggesting that they are linked by fractional crystallization of K-feldspar, plagioclase and biotite to the same or similar biotite⁷ and/or biotite-garnet granite magma.

6.4 RARE EARTH ELEMENT GEOCHEMISTRY

The rare earth element patterns from the ABB (Figure 6.8) show very high Σ REE contents relative to the Blue Tier Batholith granitoids, with the exception of the alkali feldspar granite (Higgins *et al.*, 1982). The individual granitoids of the ABB have REE patterns that are LREE enriched, HREE depleted and have negative Eu anomalies. The two anomalous analyses in Figure 6.8d are representative of the alkali feldspar granites and the related aplitic xenoliths. REE analyses of the granodiorites and micro-



granites are not available and therefore cannot be used to substantiate the differences in major and trace element compositions of these two groups of granitoids.

The alkali feldspar granites (Figure 6.8c) have very low La/Yb ratios (close to 1), large Eu anomalies and larger absolute HREE relative to the other granitoids of the ABB. Higgins *et al.* (1982) suggest that increasing hydrothermal alteration (albitization) of the alkali feldspar granites results in the decreased La/Yb ratios, lower Σ REE, and increased negative europium anomalies. The ABB alkali feldspar granites are also anomalous when compared to similar granitoids from the Blue Tier Batholith in that their absolute HREE contents are greater than other alkali feldspar granites.

6.5 GEOCHEMICAL MODELLING

Geochemical evidence suggests that the biotite-, garnet-biotite and alkali feldspar granites of the ABB may be related by fractional crystallization. This hypothesis was tested by Dr. N.C. Higgins using major and trace element geochemical models upon two of the granitoid end members. Samples 63062 and 63065 were chosen as the respective felsic amd mafic end member phases.

Major elements were used to calculate the proportions of crystallizing phases plus residual magma required to match the composition of the parent magma (63065) utilising a least-squares regression method (Wright & Doherty, 1970). Microprobe analyses of 63065 were used to represent the compositions of the early formed crystals. The trace element concentration in a magma undergoing Rayleigh fractionation were calculated using the relative proportions and total percentages of minerals crystallized (determined from the major element mixing calculations), together with their appropriate mineral-liquid distribution coefficients.

The regression analysis (Table 6.1) for the garnet-biotite and alkali feldspar trend indicates that the variation in the major elements may be due to approximately 25% fractional crystallization separating a solid composed of 64% plagioclase, 20% biotite and 16% K-feldspar. Accessory phases were not included in the petmix calculation. The negative weight fraction for K-feldspar is interpreted as resulting from incomplete separation of this cumulate mineral from a residual melt. This might imply that plagioclase and biotite were the early fractionating phases followed by K-feldspar fractionation at the final emplacement level, i.e. *in situ* fractional crystallization.

Field evidence reinforces this interpretation with the occurrence of:

- (i) K-feldspar concentrations throughout the ABB, and
- (ii) plagioclase and biotite-rich cognate (cumulate) xenoliths within the garnet-biotite granite (modal analysis #63113, Appendix 1).

Trace element calculations for the residual magma after 25% fractional crystallization of a solid (64% plagioclase, 20% biotite, 16% K-feldspar) satisfies the Sr concentration observed (40 and 39 ppm respectively). The disparity between calculated and observed Rb concentration (260 and 356 ppm respectively) suggests that the amount of biotite fractionated by the model is greater than the observed amount. The calculated Ba concentration (380 ppm) is 220 ppm above the observed value, further confirming the late *in situ* fractionation of K-feldspar. The calculated Eu concentration is higher than the true Eu concentration illustrating the importance of fractionating accessory phases (e.g. apatite, zircon, and monazite) within the granites of the ABB, since fractionation of these phases depletes a residual magma (i.e. bulk Kd > 1, Miller & Mittlefehldt, 1981).

In summary, despite some discrepancies between the calculated and observed major and trace elements, geochemical modelling illustrates the linear trend observed between the biotite-, garnet-biotite and alkali

Table 6.1

LEAST SQUARES MIXING CALCULATIONS FOR GARNET-BIOTITE AND

	Plag.	Biot.	Kfels.	63062	63065	
					observed	calculated
Si0 ₂	61.14	34.34	65.79	76.49	71.11	71.10
TiO ₂	0.00	3.69	0.00	0.14	0.28	0.31
A1203	24.58	18.47	18.59	12.29	14.23	14.35
FeO	0.00	22.18	0.00	1.61	2.52	2.49
MnO	0.00	0.00	0.00	0.02	0.03	0.02
MgO	0.00	5.48	0.00	0.10	0.44	0.38
Ca0	6.08	0.00	0.00	0.52	1.75	1.44
Na ₂ 0	7.95	0.00	1.00	2.25	3.21	3.11
к ₂ 0	0.24	8.97	14.62	5.32	4.41	4.28
P ₂ O ₅	0.00	0.00	0.00	0.07	0.13	0.06
weight fraction	0.1692	0.0541	-0.0337	0.7991		$\Sigma R^2 = 0.1462$

ALKALI FELDSPAR GRANITES

i.e. 63062 + plag + biot = 63065 + Kfels

					1
	Plag.	Biot.	Kfels.	Apatite	Zircon
Eu	2.15	0.24	1.13	30.40	3.14
Rb	0.04	2.24	0.37	0.00	0.00
Ba	0.70	9.70	6.12	0.00	0.00
Sr	5.60	0.13	3.87	0.00	0.00

KD's

i: X

The second second

feldspar granites. This is explained by approximately 25% fractional crystallization of a solid composed of plagioclase, biotite and K-feldspar.

6.6 DISCUSSION

Geochemical evidence together with geological interpretations imply that the granodiorite, microgranite and biotite-, garnet-biotite and alkali feldspar granites represent separate melts derived from various sources. Cocker (1977) infers the time span for the emplacement of the granodiorite and granites of the Blue Tier Batholith is too large (25 Ma). for *in situ* fractional crystallization of a single parent. In the Ansons Bay Batholith (ABB) the time span between granodiorite and granite, is only 13 Ma.

Geochemical modelling confirms compositional variation and similarities within the biotite-, garnet-biotite, and alkali feldspar granites. The wide linear bands observed in major and trace element trends from the Ansons Bay Batholith are the result of incomplete separation of "cumulate" and "liquid" (Tindel & Pearce, 1981), i.e. crystal mushes comprising mixtures of compositions formed along cumulate and liquid trends under Rayleigh (perfect) fractional crystallization. Modelling in fact suggests 25% fractional crystallization of a solid consisting of 64% plagioclase, 20% biotite and 16% K-feldspar. Tindel & Pearce (1981) suggest that within each magma undergoing fractional crystallization the mechanisms of crystal settling and filter pressing operated. The former being initially dominant and the latter becoming more important with increasing degrees of fractional crystallization. These respective mechanisms have been hypothesized to explain cognate (cumulate) xenoliths and K-feldspar concentrations observed in the field. Geochemical modelling of the ABB necessitates early cumulates having compositions similar to those of the cognate xenoliths, and requires the formation of K-feldspar concentrations.

White & Chappell (1977) suggest that linear geochemical trends can also be produced by restite unmixing. The features of this process are xenoliths, clots and xenocrysts in the felsic granitoids which are out of equilibrium with their enclosing rock. Re-equilibrated restites may occur. In the ABB all the igneous xenoliths are cognate and intimately associated with their host granite (Chapter 4). These have been interpreted as cumulate and are therefore not restite in origin. The zoned garnet, plagioclase and perthite crystals have petrographic features which also imply a melt origin.

Evidence for assimilation of Mathinna Beds within the ABB is restricted to an agmatic migmatite and isolated rafts of country rock and xenoliths. Cocker's (1977) estimate of 5% xenoliths in the garnetbiotite granites is correct but the majority of these xenoliths are cognate. Geochemical data show that assimilation of the Mathinna Beds is restricted to within a few metres of the agmatic migmatite.

Higgins *et al.* (1982) have, however, geochemically modelled the garnet-biotite granite of the ABB and inferred that it can be derived from the Poimena biotite granite by 10% assimilation of Mathinna Beds and 15% fractional crystallization of biotite, garnet, plagioclase and K-feldspar. This model also accounts for the Zr and Rb contents of the ABB.

In conclusion geological, petrological, mineralogical and geochemical evidence suggests the granodiorite, microgranite and biotite-, garnet-biotite, and alkali feldspar granites of the Ansons Bay Batholith were derived by Rayleigh fractional crystallization of a melt from a chemically inhomogeneous source region.

118

.

Chapter 7

SUMMARY OF CONCLUSIONS

The following is a summary of the conclusions reached in this thesis.

1. The Ansons Bay Batholith is a granitic complex (300 km^2) in northeastern Tasmania composed of a variety of granitoids which intrude and contact metamorphose low grade regionally metamorphosed Ordovician to lower Devonian Mathinna Beds.

2. The granitoids have been subdivided on the basis of mafic mineralogy, plagioclase composition and textural variation into

(i) granodiorites - Gardens Pluton Granodiorite

- Boulder Point Granodiorite

(ii) Musselroe Microgranite

(iii) biotite granites - Ansons Bay

- Eddystone Point

(iv) garnet-biotite granites - porphyritic (southern)

- coarsely porphyritic (northern)

(v) alkali-feldspar granite (Mt William).

3. Based on field relationships, petrographic features and geochemistry the granitoids are classified according to I, S-type characteristics:

I-type - granodiorites S-type - garnet-biotite granites predominantly S-type - microgranites, biotite granites and alkali feldspar granites.

4. Late Devonian dolerite dykes (up to 10 km long), lamprophyric dykes and leucocratic dykes succeeded the major granitoid intrusions. The dolerite is associated with late-stage crystallization of the granite and the lamprophyre is attributed to hybridization between basic magma and granitic residua or sediments.

5. A previously unmapped porphyritic, medium-coarse grained biotitehornblende granodiorite (Boulder Point Granodiorite) has been identified.

6. The Gardens Pluton Granodiorite formed a 1.0 to 1.5 km wide contact metamorphic aureole in the Mathinna Beds.

7. The contact between the microgranite and the garnet-biotite granite at Musselroe Point is interpreted as the incomplete mixing of two contemporaneous melts of different viscosities.

8. The Ansons Bay Batholith is divided on field observations, petrography, mineral analyses, and geochemical evidence into a northern and a southern region at Eddystone Point.

9. Planar arrangements of K-feldspar megacrysts and xenoliths form an arcuate N-S foliation around the batholith, approximately perpendicular to leucocratic dykes.

Magmatic convection resulted in biotite schlieren and biotite K-feldspar rich layers.

11. Age determinations for doleritic intrusions should provide an upper age limit to the Tabberabberan Orogeny within the Ansons Bay Batholith due to the lack of post-intrusive deformation of the granitoids following doleritic intrusions.

12. An agmatic migmatite 10-30 m wide and 300 m long suffered left lateral shearing across its contact between the garnet-biotite granite and the Mathinna Beds (raft?).

13. The K-feldspar-cordierite hornfels facies mineral assemblage of the migmatite is dependent on the original compositional banding of the country rock, and suggests P-T conditions of 1 kb and 600°C for the garnet-biotite granitic intrusion.

Martin and Antonia an

14. Contamination of the intrusive garnet-biotite granite by the country rock is restricted to within a few metres of the contact.

15. Xenoliths are a characteristic feature of the Ansons Bay Batholith and occur as either

- (i) Mathinna Bed xenoliths,
- (ii) mafic xenoliths in the granodiorite,
- (iii) porphyritic mafic xenoliths in the garnet-biotite granite, or
- (iv) aplitic xenoliths in the garnet-biotite granite.

16. The mafic xenoliths of the granodiorite have a cognate origin and are unrelated to the Mathinna Bed xenoliths, from textural and geochemical evidence.

17. The porphyritic mafic xenoliths and aplitic xenoliths of the garnetbiotite granite possess garnet-biotite (cordierite) rims which crystallized prior to the solidification of the host granite.

18. Textural and geochemical evidence suggests the mafic xenoliths of the garnet-biotite granite have a cognate origin and are unrelated to the Mathinna Bed xenoliths.

19. The similarity in hand specimen, petrography and geochemistry of the aplitic xenoliths of the garnet-biotite granite with the alkali feldspar granite, their rectangular outlines, restricted occurrence, and parallel orientation to leucocratic dykes suggest that these xenoliths are dismembered alkali feldspar dykes.

20. The inversely zones almandine-rich garnets and iron-rich mineral assemblages of the garnet-biotite granites imply the P-T conditions of emplacement were approximately 1 kb pressure and 700°C temperature.

21. Garnet-biotite (cordierite) geothermometry and feldspar geothermometry, to a lesser extent, substantiate the 700° C temperature of emplacement.

[15] A. C. Martin Manual M. C. Martin M. Ma

22. The granitoids, dolerites and lamprophyric intrusions of the Ansons Bay Batholith lie on the calcalkaline trend of Tilley (1950).

23. Geochemical evidence suggests the granitoids and related xenoliths of the Ansons Bay Batholith are non-minimum melts. The alkali feldspar granites, however, are inferred as minimum melts.

24. Major element variations show increasing SiO_2 from granodiorite, microgranite, biotite-, garnet-biotite, to alkali feldspar granite. Within this trend Fe, Al, Ti, Ca and Mg decrease. K and Na, however, increase with SiO_2 .

25. The trace elements Sr, Ba and Zr decrease regularly with increasing SiO_2 . Rb on the other hand increases with increasing SiO_2 .

26. Major and trace elements clearly separate the granodiorite from the other granitoids within the Ansons Bay Batholith. They also indicate that the microgranite may have undergone different fractionating processes relative to the biotite-, garnet-biotite, and alkali feldspar granites.

27. The geochemical trends observed in the granodiorite using fractionating vectors imply plagioclase, biotite and possibly hornblende fractionation (geochemical and petrographical evidence suggests hornblende fractionation was minimal). K-feldspar, plagioclase and biotite fractionation explain the trends observed in the biotite-, garnet-biotite, and alkali feldspar granites.

28. The granitoids of the Ansons Bay Batholith have very high Σ REE relative to the Blue Tier Batholith, excluding the alkali feldspar granites.

29. The Ansons Bay granitoids are LREE enriched, HREE depleted, and have negative Eu anomalies. The alkali feldspar granites, however, have low La/Yb ratios, large Eu anomalies, and larger absolute HREE relative to the other granitoids of the Ansons Bay Batholith due to hydrothermal alteration (albitization).

30. Major and trace element geochemical modelling illustrates the linear trend observed between the biotite-, garnet-biorite, and alkali feldspar granites, and suggests 25% fractional crystallization of a solid composed of 64% plagioclase, 20% biotite, and 16% K-feldspar.

REFERENCES

Abbott, R.N., and Clarke, D.B., 1979: Hypothetical liquidus relationships in the subsystem Al₂O₃- FeO-MgO projected from quartz, alkali feldspar and plagioclase for a(H₂O) < 1. *Cadnadian Mineralogist*, 17, 549-560.

Augustithis, S.S., 1973: Atlas of the tectural patterns of granites, gneisses and associated rock types. Elsevier Scientific Publishing Company, New York.

Banks, M.R., 1962a: Permian System, in Geology of Tasmania. J. Geol. Soc. Aust., 9, 189-215.

Banks, M.R., 1962: Mathinna Beds. in Geology of Tasmania. J. Geol. Soc. Aust., 9, 182-185.

Barriere, M., 1981: On curved laminae, graded layers, convection currents and dynamic crystal sorting in the Ploumanac'h (Brittany) subalkaline granite. *Contrib. Mineral. Petrol.*, 77, 214-224.

Bateman, P.C., and Dodge, F.C.W., 1970: Variations in major chemical constituents across the Central Sierra Nevada Batholith. *Geol. Soc. Am. Bull.*, 81, 409-420.

Brown, W.L., and Parsons, I., 1981: Towards a more practical two feldpsar geothermometer. Contrib. Mineral. Petrol., 76, 369-377.

Carmichael, I.S.E., Turner, F.J., and Verhoogen, J., 1974: Igneous Petrology. McGraw-Hill, New York.

Chappell, B.W., and White, A.J.R., 1974: Two contrasting granite types. Pac. Geol., 8, 173-174.

Cocker, J.D., 1971: The St Helens Pluton. Petrológy and structure. Unpub. B.Sc. Honours thesis, University of Tasmania.

Cocker, J.D., 1977: Petrogenesis of the Tasmanian granitoids. Unpub. Ph.D. thesis, University of Tasmania.

Cocker, J.D., 1981: Petrogenesis of garnet and cordierite granites from Tasmania, Australia. Contrib. Mineral. Petrol., 78,

Cocker, J.D., 1982: Rb-Sr geochronology and Sr isotopic composition of Devonian granitoids, eastern Tasmania. J. Geol. Soc. Aust., 29, 139-158.

Dietvorst, E.J.L., 1982: Retrograde garnet zoning at low water pressure in metapelitic rocks from Kemio, S.W. Finland. *Contrib. Mineral. Petrol.*, 79, 37-45.

Eby, G.N., 1972: Determination of rare-earth yttrium and scandium abundances in rocks and minerals by an ion exchange X-ray fluorescence procedure. Anal. Chem., 44, 2137-2143.

- Emmermann, R., Daieva, L., and Schneider, J., 1975: Petrologic significance of rare earths distribution in granites. *Contrib. Mineral. Petrol.*, 52, 267-283.
- Ferry, J.M., and Spear, F.S., 1978: Experimental calibration of the partitioning of Fe and Mg between biotite and garnet. *Contrib. Mineral. Petrol.*, 66, 113-117.
- Fourcade, S., and Allegre, C.J., 1981: Trace element behaviour in granite genesis: a case study. The calc-alkaline plutonic association from the Querigut Complex (Pyrenees, France). Contrib. Mineral. Petrol., 76, 177-195.
- Froese, E., 1973: The assemblage quartz-Kfeldspar-biotite-garnetsillimanite as an indicator of $P(H_2O)$ -T conditions. Can. J. Earth Science, 10, 1575-1579.
- Fryer, B.J., 1977: Rare earth evidence in iron formations for changing Precambrian oxidation states. Geochim. Cosmochim. Acta, 41, 361-367.
- Fyfe, W.S., Turner, F.J., and Verhoogen, J., 1958: Metamorphic reactions and metamorphic facies. *Geol. Soc. Am. Mem.*, 73, 1-252.
- Gee, R.D., and Groves, D.I., 1971: Structural features and mode of emplacement of part of the Blue Tier Batholith in North-East Tasmania. Jour. Geol. Soc. Aust., 18, 41-56.
- Groves, D.I., 1972: Geochemical evolution of tin-bearing granites in the Blue Tier Batholith, Tasmania. *Econ. Geol.*, 67, 445-457.
- Groves, D.I., Cocker, J.D., Jennings, D.L., and McShane, R., 1977: The Blue Tier Batholith. *Geol. Surv. Bull. Tasm. 55.*
- Groves, D.I., and McCarthy, T.S., 1978: Fractional crystallization and the origin of tin deposits in granitoids. *Mineral. Deposita*, *(Berl.)*, 13, 11-26.
- Harker, A., 1939: Metamorphism: a study of the transformation of rock masses. Methuen, London.
- Higgins, N.C., Solomon, M., and Varne, R., 1982: The genesis of the granitoids of the Blue Tier Batholith, N.E. Tasmania. (in prep.)
- Hine, R., Williams, I.S., Chappell, B.W., and White, A.J.R., 1978: Contrasts between I- and S-type granitoids of the Koscuisko Batholith. J. Geol. Soc. Aust., 25, 219-234.
- Jennings, D.J., 1977: The search for tin at Mount William. Bull. Geol. Surv. Tasm. 55, 157-171.
- Marshall, B., 1969: Explanatory Report. 1-Mile geological map series. Pipers River. Department of Mines, Tasmania.

125

÷.

and the second

1917 - 19

McCarthy, T.S., and Groves, D.I., 1979: The Blue Tier Batholith, North-Eastern Tasmania: a cumulate-like product of fractional crystallization. *Contrib. Mineral. Petrol.*, 71, 193-209.

McClenaghan, M.P., and Baillie, P.W., 1975: Launceston, SK-55/4. Explan. Report, Department of Mines, Tasmania.

McClenaghan, M.P., and Williams, P.R., 1982: Distribution and characterisation of granitoid intrusions in the Blue Tier area. Tas. Dept. Mines. Geol. Surv. Paper 4.

Miller, C.F., and Mittlefelhdt, D.W., 1982: Depletion of light rareearth elements in felsic magmas. *Geology*, 10, 129-133.

- Norrish, K., and Hutton, J.T., 1969: An accurate X-ray spectrographic method for the analysis of a wide range of geological samples. *Geochem. Cosmochim. Acta*, 33, 431-453.
- Parker, R.L., 1967: Composition of the Earth's crust, in Data of geochemistry. Fleischer, M. (ed.). U.S. geol. Surv. Prof. Paper 440-D.
- Pitcher, W.S., 1979: The nature, ascent and emplacement of granitic magmas. J. Geol. Soc. London, 136, 627-662.
- Rickards, R.B., and Banks, M.R., 1979: An early Devonian monograptid from the Mathinna Beds, Tasmania. *Alcheringa*, *3*, 307-311.
- Rock, N.M.S., 1977: The nature and origin of lamprophyres: some definitions, distinctions and derivations. *Earth Science Reviews*, 13, 123-169.

Sederholm, J.J., 1967: Selected works: granites and migmatites.

Oliver and Boyd, Edinburgh.

Skrezeczynski, R., 1971: The Bridport Granodiorite and its contact aureole. Unpub. B.Sc. Honours thesis, University of Tasmania.

- Solomon, M., 1963: Counting and sampling errors in modal analysis by point counting. *Jour. Petrol.*, 4, 367-382.
- Solomon, M., and Green, R., 1966: A chart for designing modal analysis by point counting.

Solomon, M., and Griffiths, J.R., 1972: Tectonic evolution of the Tasman Orogenic Zone, eastern Australia. *Nature*, 237, 3-6.

Solomon, M., and Griffiths, J.R., 1974: Aspects of the early history of the Southern Tasman Orogenic Zone, in The Tasman Geosyncline a Synposium. Geol. Soc. Aust. Spec. Pub., 19-46.

Streckeisen, A., 1976: To each plutonic rock its proper name.

Earth Science Reviews, 12, 1-33.

- Thompson, A.B., 1976: Mineral reactions in pelitic rocks: 1. Prediction of P-T-X (Fe-Mg) phase relations. Am. J. Sci., 276, 401-424.
- Turner, F.J., 1968: Metamorphic petrology mineralogical and field aspects. McGraw-Hill, New York.
- Van Moort, J.C., 1966: Les roches cristallophyll des Cevennes et les roches plutoniques de Mont Lozere. Ann. Fac. Sci. Univ. Clermont, 31, 272 pp.
- White, A.J.R., and Chappell, B.W., 1977: Ultrametamorphism and granitoid genesis. *Tectonophysics*, 43, 7-22.
- Winkler, H.G.F., 1965: Petrogenesis of metamorphic rocks. Springer-Verlag, Berlin.
- Wright, T.L., and Doherty, P.C., 1970: A linear programming and least squares computer method for solving petrologic mixing problems. Bull. Geol. Soc. Am., 81, 1995-2008.

(